Supporting Information

**Table of contents**

1 Syntheses ... 2
1.1 Ligand Syntheses ... 2
1.1.1 2,7-Di((pyridin-3'-yl)ethynyl)-10-hexylacrid-9-one(3) ... 2
1.1.2 2-Cyano-2-(2,7-di[(pyridin-3-yl)ethynyl)]10-hexyl-9-acridinylidene)ethylacetate $L^{Et}$ (5) ... 3
1.1.3 2-Cyano-2-(2,7-di[(pyridin-3-yl)ethynyl)]10-hexyl-9-acridinylidene)*tert*-butylacetate $L^{tBu}$ (6) ... 5
1.1.4 2-Cyanophenylacetate (7) ... 7
1.1.5 2-Cyano-2-(2,7-di[(pyridin-3-yl)ethynyl)]10-hexyl-9-acridinylidene)phenylacetate $L^{Ph}$ (8) ... 7
1.1.6 2-(2,7-Di[(pyridin-3-yl)ethynyl)]10-hexyl-9-acridinylidene)malononitrile $L^{CN}$ (9) ... 9
1.1.7 UV/Vis spectra of $L^{Et}$, $L^{tBu}$, $L^{Ph}$ and $L^{CN}$ ... 11
1.1.8 2-cyano-2-(10-hexyl-9-acridinylidene)ethylacetate (15) ... 12
1.2 Cage Syntheses ... 14
1.2.1 $[Pd_2L^{Et}_4](BF_4)_4$ (10) ... 14
1.2.3 $[Pd_2L^{Ph}_4](BF_4)_4$ (12) ... 16
1.2.4 $[Pd_2L^{CN}_4](BF_4)_4$ (13) ... 17
1.2.5 ESI-MS spectra of $[Pd_2L^{Et}_4](BF_4)_4$, $[Pd_2L^{tBu}_4](BF_4)_4$ and $[Pd_2L^{Ph}_4](BF_4)_4$ ... 18
1.2.6 Solvent effect on the NMR chemical shifts of ligand $L^{Et}$ and the $[Pd_2L^{Et}_4]$ cage ... 19
2 Variable Temperature NMR Experiments of ligands ... 20
2.1 VT-NMR of $L^{Et}$ ... 20
2.2 VT-NMR of $L^{tBu}$ ... 21
2.3 VT-NMR of $L^{Ph}$ ... 22
2.4 Comparison VT-NMR of Ligand $L^{Et}$ and Backbone $B^{Et}$ ... 23
2.5 VT-NMR of $B^{Et}$ ... 24
2.6.1 VT-NMR vs. DNMR3 Simulation of a/a' signals in $B^{Et}$ ... 25
2.6.2 Eyring plot of rotation constants extracted from VT $^1$H-NMR experiments ... 26
2.6.3 Eyring plot of rotation constants extracted from DNMR simulations ... 27
2.5 Rotation and flipping in ligand and cage ... 28
3 Guest Titration NMR Experiments ... 29
3.1 Titration of $[Pd_2L^{Et}_4]$ cage with bis-anionic guests ... 29
3.1.1 Titration of $[Pd_2L^{Et}_4]$ cage with $G^1$ ... 30
3.1.2 Titration of $[Pd_2L^{Et}_4]$ cage with $G^2$ ... 31
3.1.3 Titration of $[Pd_2L^{Et}_4]$ cage with $G^3$ ... 32
3.1.4 Titration of $[Pd_2L^{Et}_4]$ cage with $G_4$ ... 33
3.1.5 Titration of $[Pd_2L^{Et}_4]$ cage with $G_5$ ... 34
3.2 Solvent and temperature influence on $G_5$@$[Pd_2L^{Et}_4]$ host -guest complex ... 35
3.2.1 $G_5$@$[Pd_2L^{Et}_4]$ host -guest complex in DMSO at rt ... 35

3.2.2 Influence of solvent and temperature on host-guest complexes $G_5$@[$Pd_2L^{Et}_4$] ..... 36
3.2.3 $G_5$@[$Pd_2L^{Et}_4$] host-guest complex in MeOH at 60°C ..... 37
3.2.4 $G_5$@[$Pd_2L^{Et}_4$] host-guest complex in $MeNO_2$ at 60°C ..... 38
3.2.5 $G_5$@[$Pd_2L^{Et}_4$] host-guest complex in DMSO at 60°C ..... 39
4 X-Ray crystal structures ..... 40
4.1 Table ..... 40
5 Computational Studies ..... 41

# 1 Syntheses

## 1.1 Ligand Syntheses

All reactions were carried out under inert conditions unless mentioned otherwise. All compounds were synthesized from commercially available chemicals. All GPC purifications were performed on a JAI 9210-II NEXT GPC System with a JAIGEL HH-2/HH-1 column combination running with $CHCl_3$ (HPLC grade, stabilized with Ethanol, VWR).

### 1.1.1 2,7-Di((pyridin-3'-yl)ethynyl)-10-hexylacrid-9-one(3)

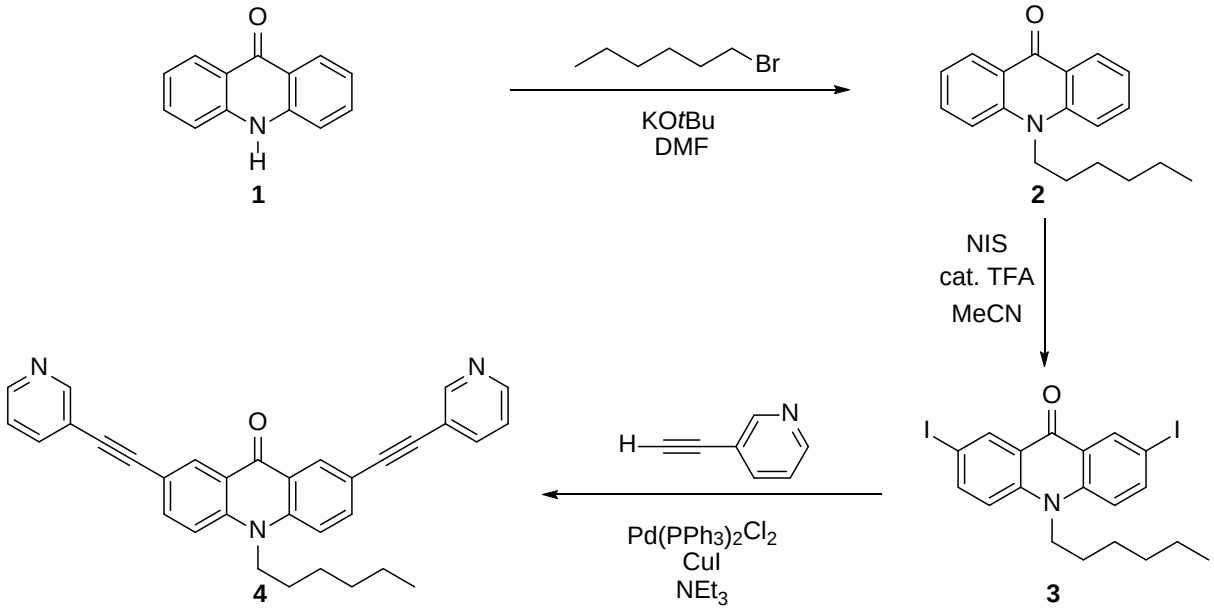


Compound **4** was synthesized as described previously[1] from 9(10H)-Acridone (**1**) by introducing a hexyl residue to the acridone nitrogen to give **2** followed by double iodination at 2- and 7-postion and Sonogashira cross-coupling to attach the pyridine arms to give **3.**

### 1.1.2 2-Cyano-2-(2,7-di[(pyridin-3-yl)ethynyl)]10-hexyl-9-acridinylidene)ethylacetate $L^{Et}$ (5)

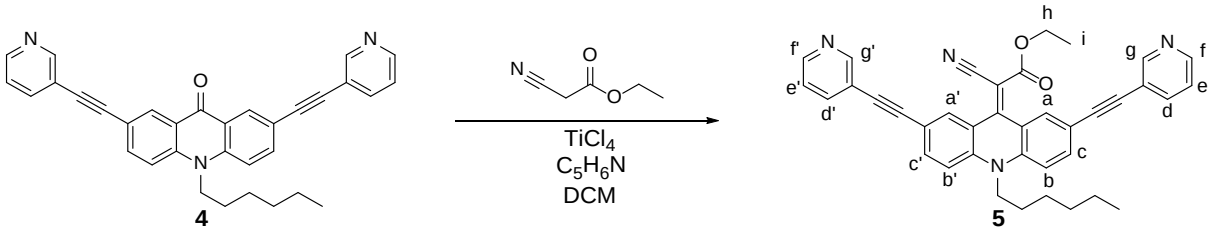


$TiCl_4$ (255 mg, 1.34 mmol, 1.25 equiv.) was slowly added to **4** (300 mg, 1.07 mmol, 1.00 equiv.) dissolved in dry $CH_2Cl_2$ (15 mL) and stirred for 15min at room temperature. 2-Cyanoethylacetate (244 mg, 2.15 mmol, 2.00 equiv.) and $NEt_3$ (2 mL) were added consecutively to the reaction mixture and heated to 70°C under reflux for 24 h. The cooled down reaction mixture was filtered through celite and the residue was washed with $CH_2Cl_2$ (2 x 50mL). The solvent was removed *in vacuo* and the residue was purified by column chromatography ($SiO_2$, chloroform/methanol 40:1 → 20:1) followed by purification via GPC. The product (481 mg, 0.83 mmol, 78%) was obtained as a red solid.

**$^1$H-NMR** (400 MHz, 298 K, $CDCl_3$): $\delta$ (ppm) = 8.78 (s, 2H, g/g'), 8.60 (dd, $^3J$ = 5.0, $^4J$ = 1.7 Hz, 2H, f/f'), 7.86 (dt, $^3J$ = 7.9,$^4J$= 2.0 Hz, 2H, d/d'), 7.72 (dd, $^3J$ = 9.0, $^4J$= 2.0 Hz, 2H, c/c'), 7.34 (d, $^3J$ = 8.9 Hz, 2H, b/b'), 7.34 (dt,$^3J$ = 7.9,$^4J$ = 4.8 Hz,2H, e/e*), 4.30 (q, $^3J$ = 7.2 Hz, 2H, h), 4.24 - 4.18 (, 2H, NC$\underline{H}_2$), 2.01 - 1.88 (m, 2H, C$\underline{H}_2$), 1.59 - 1.48 (m, 2H, C$\underline{H}_2$), 1.47 - 1.33(m, 4H, C$\underline{H}_2$C$\underline{H}_2$CH$_3$), 1.31 (t, $^3J$ = 7.1 Hz, 3H, i), 0.94 (t, $J$ = 7.0 Hz, 3H, C$\underline{H}_3$).

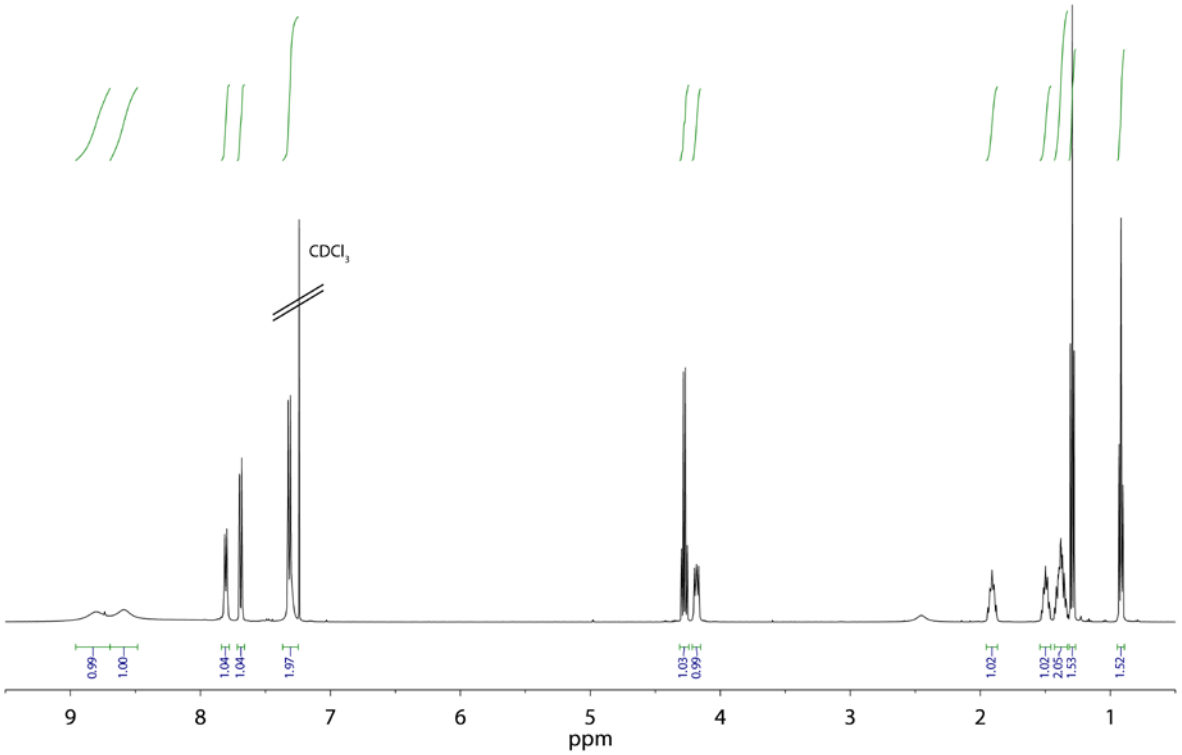


**$^{13}$C-NMR** (176 MHz, 298 K, $CDCl_3$): $\delta$ (ppm) = 164.6, 151.6, 149.7, 147.9, 139.5, 138.9, 134.9, 123.5, 118.3, 115.6, 114.2, 94.7, 91.9, 86.6, 77.25, 62.3, 47.8, 31.4, 26.6, 26.5, 24.6, 22.6, 14.1, 14.0.

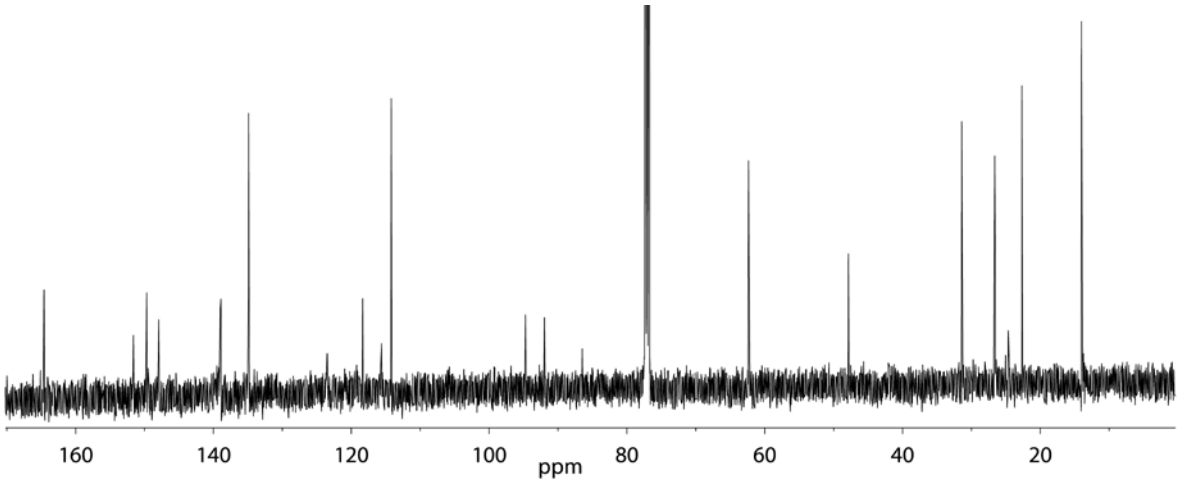


**UV/Vis (MeCN):** $\lambda_{max}$ ($\varepsilon$)=272 (48000), 340 (44600), 472 (10600)

**IR (ATR):** $\tilde{\nu}$ ($cm^{-1}$) = 2926, 2207, 1716, 1522, 1478, 1465, 1372, 1235, 1183, 1102, 1021, 823, 804, 702.

**Melting point:** 148-149 °C

| | | | | |
|---|---|---|---|---|
| **ESI-HRMS** ($[C_{38}H_{32}N_4O_2]^+$): | measured: | 577.2577 | | |
| | calculated: | 577.2598 | | |
| **Elemental analysis:** ($C_{38}H_{32}N_4O_2 \cdot H_2O$) | calculated: | %C 76.7 | %H 5.8 | %N 9.4 |
| | found: | %C 76.3 | %H 5.9 | %N 9.2 |

### 1.1.3 2-Cyano-2-(2,7-di[(pyridin-3-yl)ethynyl)]10-hexyl-9-acridinylidene)*tert*-butylacetate L$^{tBu}$ (6)

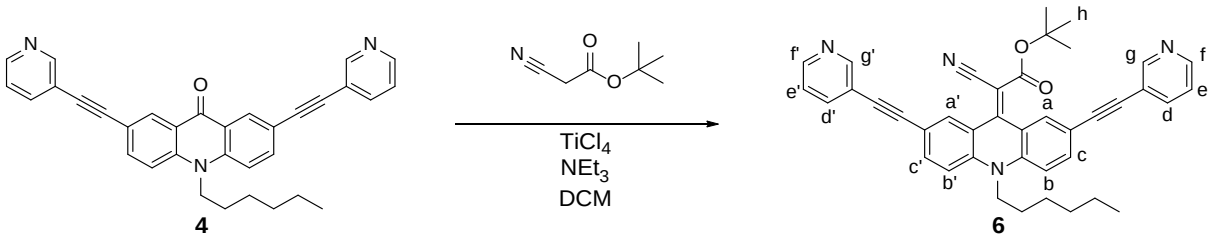


$TiCl_4$ (255 mg, 1.34 mmol, 1.25 equiv.) was slowly added to **4** (300 mg, 1.07 mmol, 1.00 equiv.) dissolved in dry $CH_2Cl_2$ (15 mL) and stirred for 15 min at room temperature. 2-Cyano-*tert*-butylacetate (304 mg, 2.15 mmol, 2.00 equiv.) and $NEt_3$ (2 mL) were added consecutively to the reaction mixture and heated to 70°C under reflux for 24 h. The cooled down reaction mixture was filtered through celite and the residue was washed with $CH_2Cl_2$ (2 x 50mL). The solvent was removed *in vacuo* and the residue was purified by means of column chromatography ($SiO_2$, chloroform/methanol 40:1 → 20:1) followed by purification via GPC. The product (214 mg, 0.36 mmol, 33%) was obtained as an orange solid.

**$^1$H-NMR** (300 MHz, 298 K, $CDCl_3$): $\delta$ (ppm) 8.74 (s, 2H, g/g'),8.71 (s, 1H, a'), 8.54 (dd, $^3J$ = 5.0, $^4J$ = 1.7 Hz, 2H, f/f'), 7.80 (dt, $^3J$ = 7.9,$^4J$= 2.0 Hz, 2H, d/d'), 7.76 (s, 1H, a), 7.69 (dd, $^3J$ = 9.0, $^4J$= 2.0 Hz, 2H, c/c'), 7.29 (d, $^3J$ = 8.9 Hz, 2H, b/b'), 7.28 (dt,$^3J$ = 7.9,$^4J$ = 4.8 Hz,2H, e/e*), 4.23 – 4.09 (m, 2H, NC$\underline{H}_2$), 1.90 – 1.81 (m, 2H, C$\underline{H}_2$), 1.48 (s, 9H, h), 1.51 – 1.45 (m, 2H, C$\underline{H}_2$), 1.43 – 1.32 (m, 4H, C$\underline{H}_2$C$\underline{H}_2$CH$_3$), 0.93(t, $J$ = 7.0 Hz, 3H, C$\underline{H}_3$).

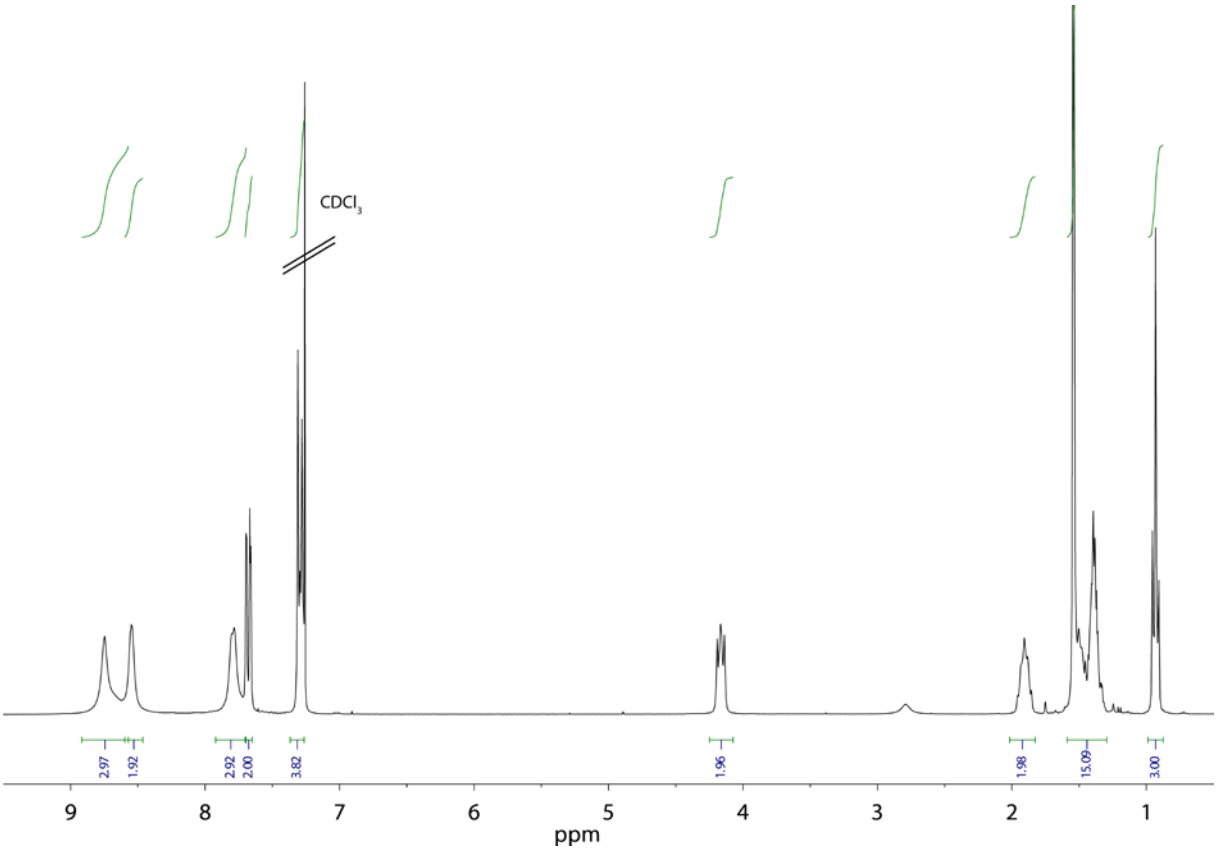

**$^{13}$C-NMR** (176 MHz, 298 K, $CDCl_3$): $\delta$ (ppm) = 163.7, 151.7, 148.2, 147.7, 139.1, 138.7, 134.7, 132.7, 129.9, 123.6, 118.4, 114.2, 97.3, 92.1, 86.6, 83.9, 47.8, 31.5, 29.8, 27.9, 26.7, 26.6, 22.8, 14.1

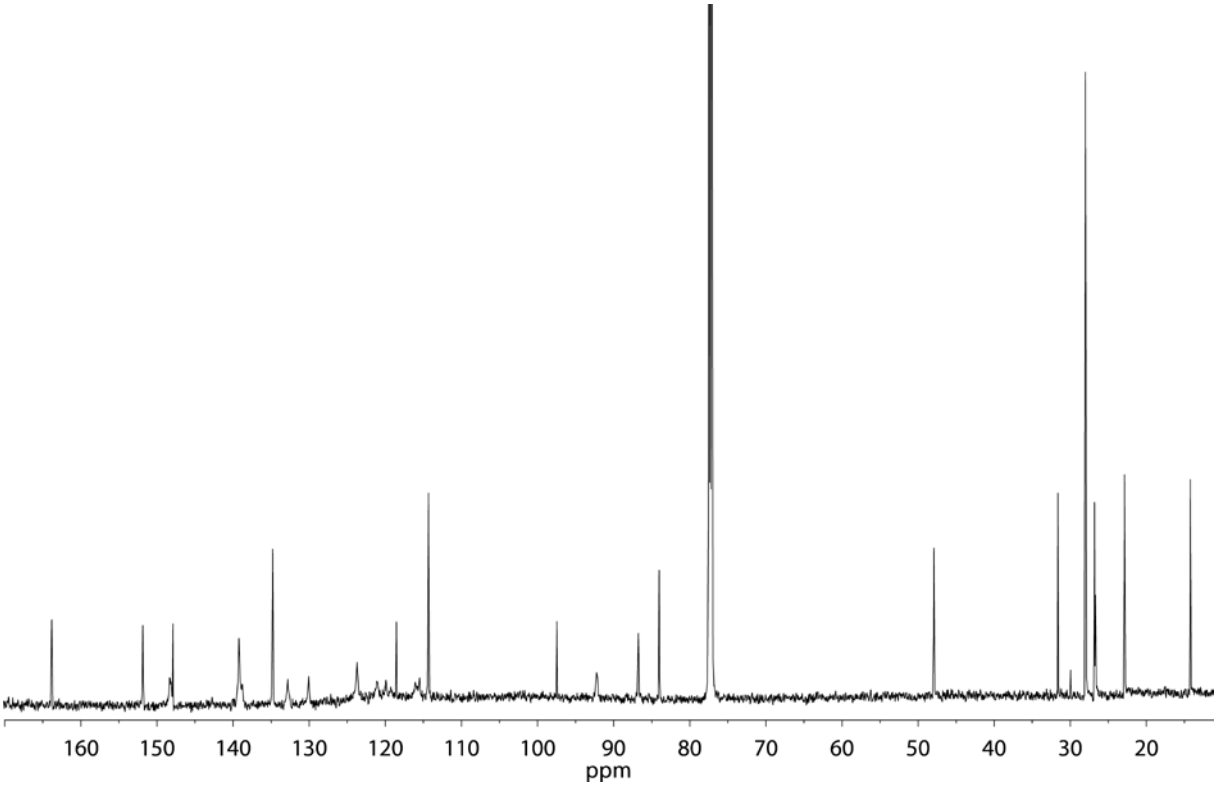


**UV/Vis (MeCN):** $\lambda_{max}$ ($\varepsilon$)=273 (45900), 367 (38800), 466 (9800).

**IR (ATR):** $\tilde{\nu}$ ($cm^{-1}$) = 2932, 2198, 1719, 1575, 1481, 1460, 1370, 1250, 1163, 1144, 1105, 1022, 840, 801, 702.

**Melting point:** 169-170 °C

| | | | | |
|---|---|---|---|---|
| **ESI-HRMS** ($[C_{40}H_{37}N_4O_2]^+$): | measured: | 605.2838 | | |
| | calculated: | 605.2822 | | |
| **Elemental analysis:** ($C_{40}H_{37}N_4O_2 \cdot H_2O$) | calculated: | %C 77.2 | %H 6.2 | %N 9.0 |
| | found: | %C 77.6 | %H 6.1 | %N 8.9 |

### 1.1.4 2-Cyanophenylacetate (7)

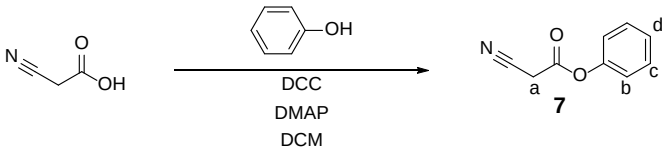


2-Cyanoacetic acid (1.00 g, 11.76 mmol, 1.00 equiv.), phenol (1.22 g, 12.93 mmol, 1.10 equiv.) 4,4'-dimethylaminpyridine (143 mg, 1.18 mmol, 0.10 equiv.) and *N,N'*-dicyclohexyl carbodiimide (2.67 g, 12.93 mmol, 1.10 equiv.) in $CH_2Cl_2$ (15 mL) were stirred at 0 °C. The reaction mixture was allowed to warm up to room temperature over 12 h. After that the reaction mixture was filtered through celite and the solvent was removed *in vacuo*. The residue was purified by means of column chromatography (SiO2, pentane/ethyl acetate 6:1→2:1). The product (1.53 g, 9.50 mmol, 81%) was obtained as red oil.

**$^1$H-NMR** (300 MHz, 298 K, $CD_3CN$): $\delta$ (ppm) = 7.47 – 7.38 (m, 2H, c), 7.35 – 7.29 (m, 1H, d), 7.19 – 7.13 (m, 2H, b), 3.73 (s, 2H, a).

### 1.1.5 2-Cyano-2-(2,7-di[(pyridin-3-yl)ethynyl)]10-hexyl-9-acridinylidene)phenylacetate $L^{Ph}$ (8)

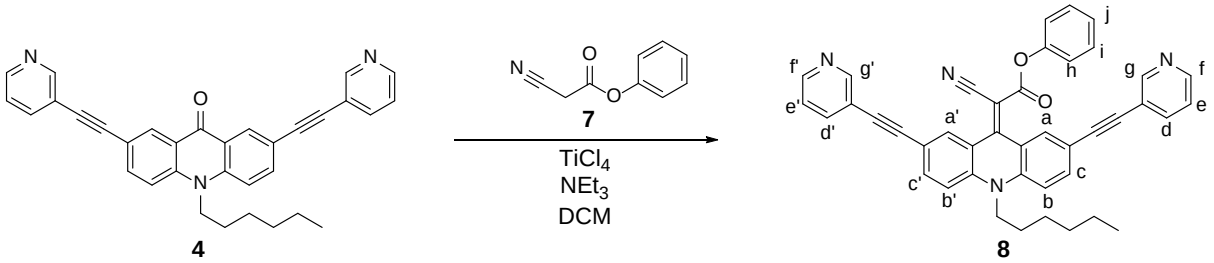


$TiCl_4$ (255 mg, 1.34 mmol, 1.25 equiv.) was slowly added to **4** (300 mg, 1.07 mmol, 1.00 equiv.) solved in dry $CH_2Cl_2$ (15 mL) and stirred for 15min at room temperature. **7** (346 mg, 2.15 mmol, 2.00 equiv.) and $NEt_3$ (2 mL) were added consecutively to the reaction mixture and heated to 70°C under reflux for 24 h. The cooled down reaction mixture was filtered through celite and the residue was washed with $CH_2Cl_2$ (2 x 50mL). The solvent was removed *in vacuo* and the residue was purified by means of column chromatography ($SiO_2$, chloroform/methanol 40:1 → 20:1) followed by purification via GPC. The product (153 mg, 0.25 mmol, 23%) was obtained as a dark red solid.

**$^1$H-NMR** (400 MHz, 298 K, $CDCl_3$): $\delta$ (ppm) 8.76 (s, 2H, g/g'), 8.57 (dd, $^3J$ = 5.0, $^4J$ = 1.7 Hz, 2H, f/f'), 8.42 (d, $^4J$ = 2.0 Hz, 2H, a/a'), 7.90 (dt, $^3J$ = 7.9,$^4J$= 2.0 Hz, 2H, d/d'), 7.82 (dd, $^3J$ = 9.0, $^4J$= 2.0 Hz, 2H, c/c'), 7.65 (d, $^3J$ = 8.9 Hz, 2H, b/b'), 7.41 – 7.35 (m, 4H, e/e*, i), 7.27 – 7.23 (m, 1H, j), 7.22 – 7.18 (m, 2H, h), 4.37 – 4.30 (m, 2H, $NC\underline{H}_2$), 1.92 – 1.83 (m, 2H, $C\underline{H}_2$), 1.52 – 1.45 (m, 2H, $C\underline{H}_2$), 1.42 – 1.30 (m, 4H, $C\underline{H}_2C\underline{H}_2CH_3$), 0.90 (t, $J$ = 7.0 Hz, 3H, $C\underline{H}_3$).

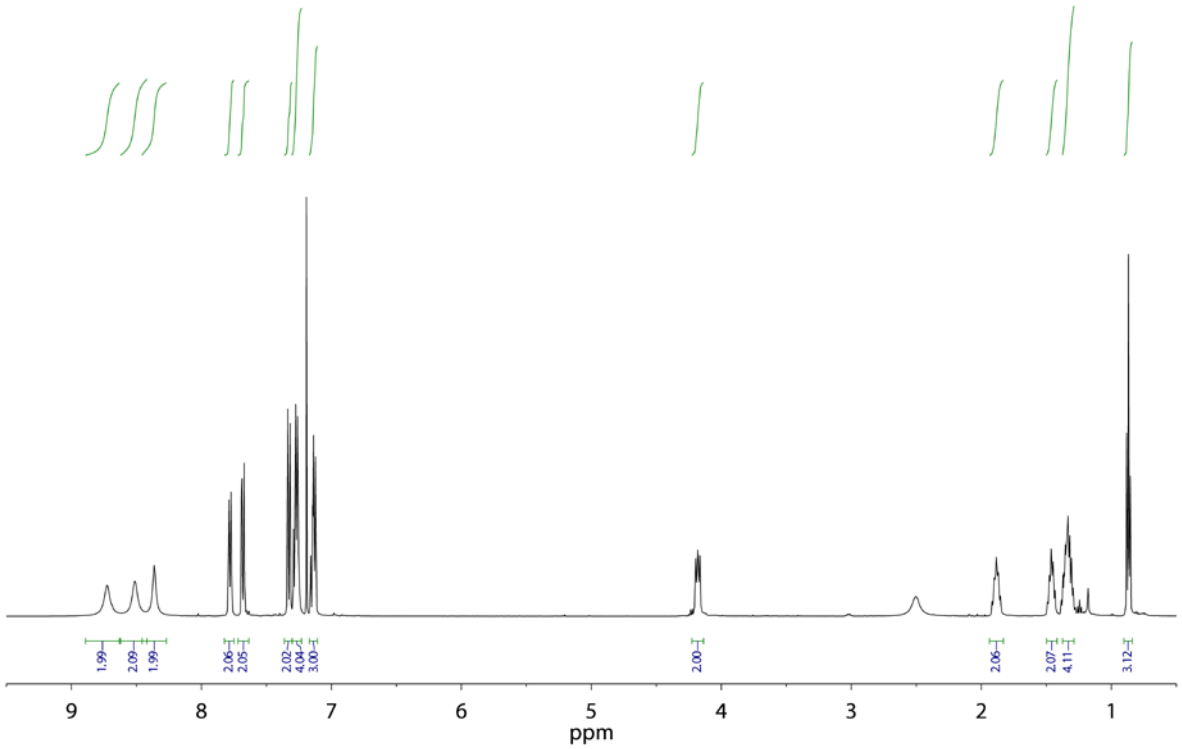


**$^{13}$C-NMR** (176 MHz, 298 K, $CDCl_3$): $\delta$ (ppm) = 163.7, 151.7, 148.2, 147.7, 139.1, 138.7, 134.7, 132.7, 129.9, 123.6, 118.4, 114.2, 97.3, 92.1, 86.6, 83.9, 47.8, 31.5, 29.8, 27.9, 26.7, 26.6, 22.8, 14.1.

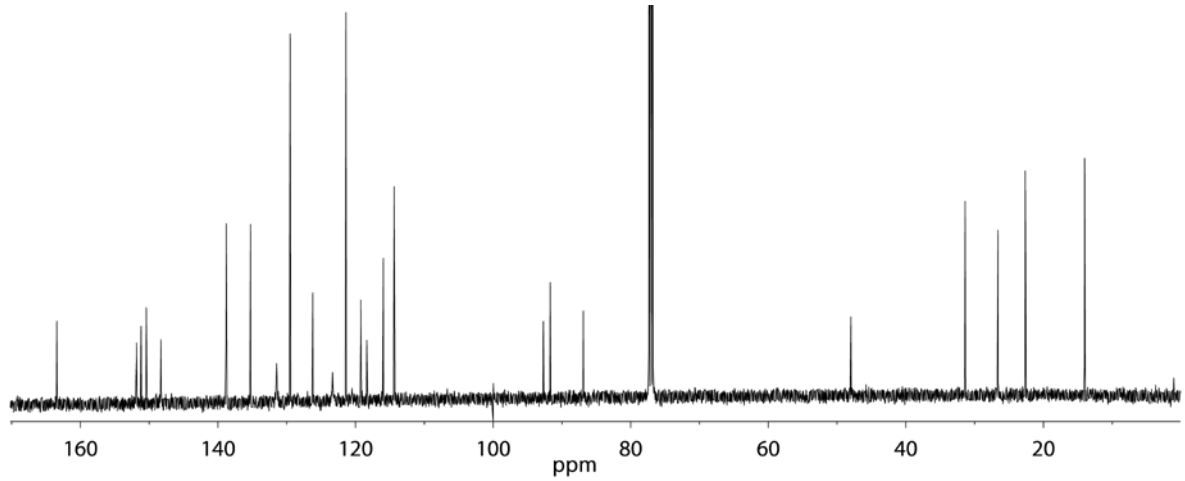


**UV/Vis (MeCN):** $\lambda_{max}$ ($\varepsilon$)=273 (38500), 345 (42900), 489 (9600).

**IR (ATR):** $\tilde{\nu}$ ($cm^{-1}$) = 2931, 2183, 1716, 1564, 1480, 1468, 1410, 1370, 1267, 1176, 1165,1079, 810, 748, 703

| | | | | |
|---|---|---|---|---|
| **ESI-HRMS**($[C_{42}H_{33}N_4O_2]^+$): | measured: | 625.2583 | | |
| | calculated: | 625.2525 | | |
| **Elemental analysis:** ($C_{42}H_{32}N_4O_2 \cdot H_2O$) | calculated: | %C 78.5 | %H 5.4 | %N 8.7 |
| | found: | %C 78.3 | %H 5.8 | %N 9.0 |

### 1.1.6 2-(2,7-Di[(pyridin-3-yl)ethynyl)]10-hexyl-9-acridinylidene)malononitrile $L^{CN}$ (9)

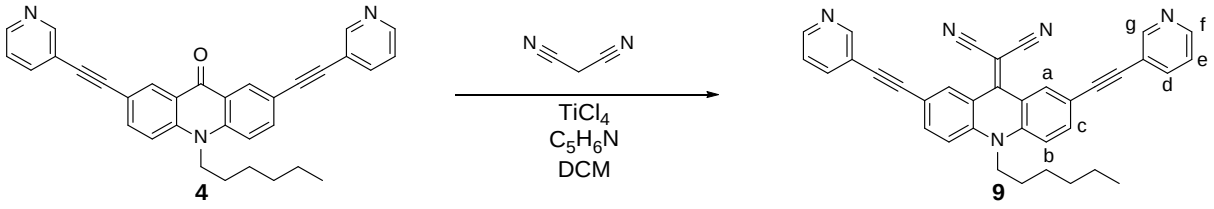


$TiCl_4$ (255 mg, 1.34 mmol, 1.25 equiv.) was slowly added to **4** (300 mg, 1.07 mmol, 1.00 equiv.) dissolved in dry $CH_2Cl_2$ (15 mL) and stirred for 15min at room temperature. Malononitrile (142 mg, 2.15 mmol, 2.00 equiv.) and $NEt_3$ (2 mL) were added consecutively to the reaction mixture and heated to 70°C under reflux for 24 h. The cooled down reaction mixture was filtered through celite and the residue was washed with $CH_2Cl_2$ (2 x 50mL). The solvent was removed *in vacuo* and the residue was purified by column chromatography ($SiO_2$, chloroform/methanol 40:1 → 20:1) followed by purification via GPC. The product (482 mg, 0.91 mmol, 85%) was obtained as an orange solid.

**$^1$H-NMR** (400 MHz, 298 K, $CDCl_3$): $\delta$ (ppm) = 8.77 (dd, $^4J$ = 2.2 Hz, 2H,g), 8.61 (d, $^4J$ = 1.9 Hz, 2H, a), 8.57 (dd, $^3J$ = 4.9, $^4J$ = 1.7 Hz, 2H, f), 7.92 (dt, $^3J$ = 7.9,$^4J$= 2.0 Hz, 2H, d), 7.90 (dd, $^3J$ = 3.7, $^4J$ = 1.9 Hz, 2H, c), 7.72 (d, $^3J$ = 9.1 Hz, 2H, b), 7.40 (dd, $^3J$ = 7.9, $^4J$ = 4.9, 2H, e), 4.44 – 4.31 (m, 2H, $NC\underline{H}_2$), 1.95 – 1.83 (m, 2H, $C\underline{H}_2$) 1.61 – 1.44 (m, 2H, $C\underline{H}_2$), 1.43 – 1.32 (m, 4H, $C\underline{H}_2C\underline{H}_2CH_3$), ), 0.94 (t, $J$ = 7.0 Hz, 3H, $C\underline{H}_3$).

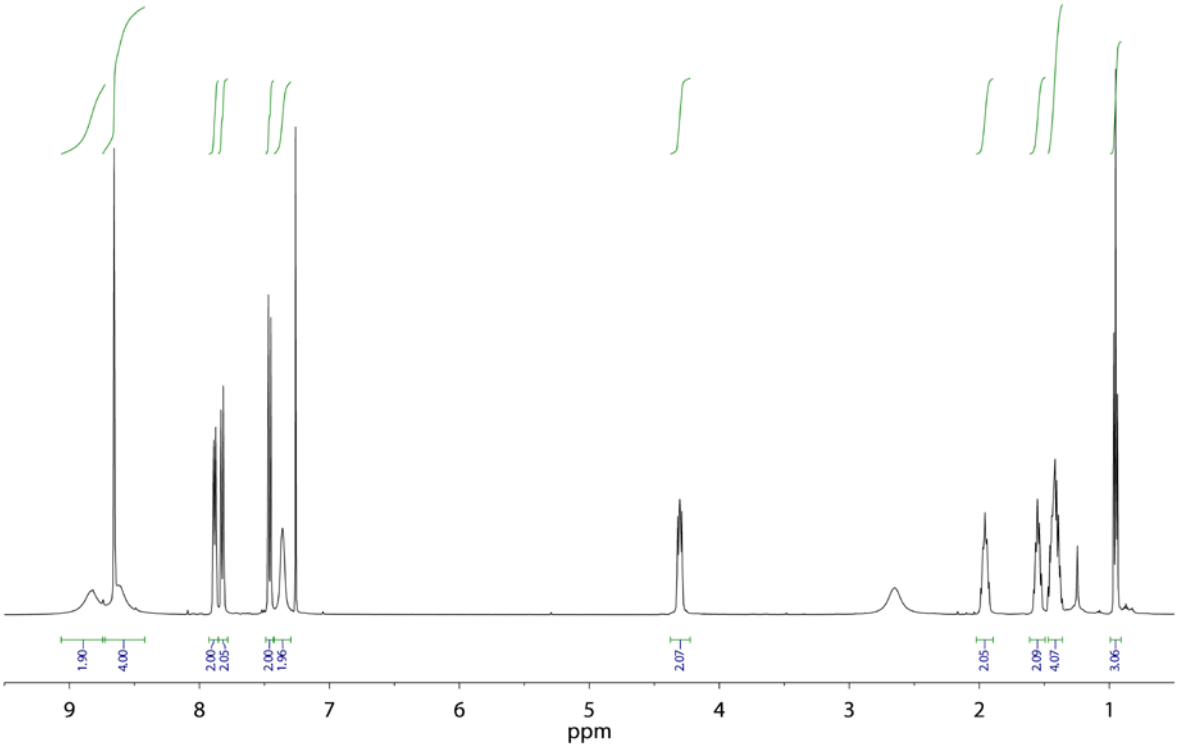

**$^{13}$C-NMR** (176 MHz, 298 K, $CDCl_3$): $\delta$ (ppm) = 154.4, 151.8, 148.3, 139.2, 138.5, 136.5, 130.3, 123.5, 118.2, 116.8, 116.6, 114.9, 91.33, 87.49, 77.4, 70.7, 48.4, 31.5, 26.9, 26.7, 22.7, 14.1.

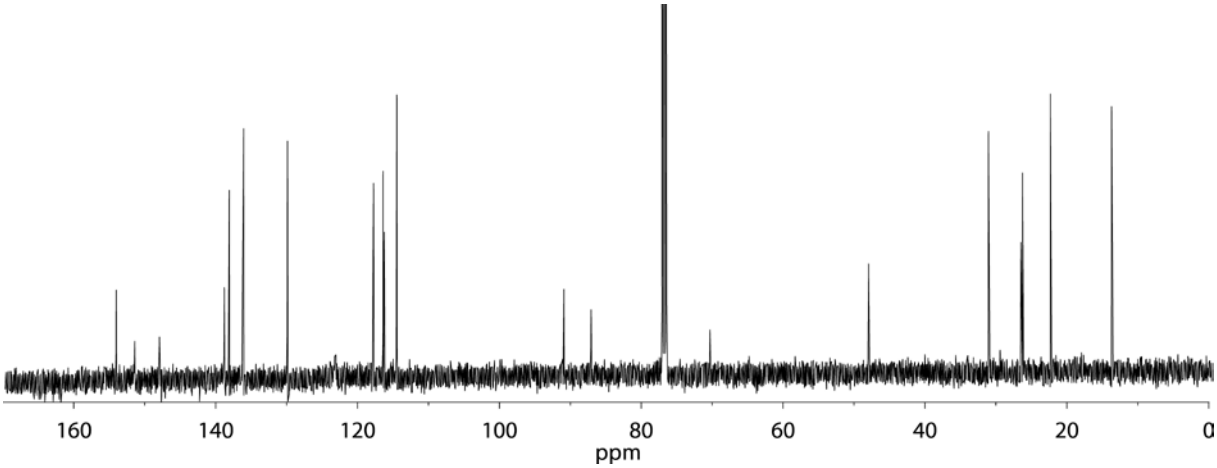


**UV/Vis (MeCN):** $\lambda_{max}$ ($\varepsilon$)=287 (48500), 347 (62300), 505 (16000).

**IR (ATR):** $\tilde{\nu}$ ($cm^{-1}$) = 2924, 2854, 2206, 1562, 1480, 1465, 1368, 1263, 1186, 1021, 895, 820, 806, 702, 627, 588.

**Melting point:** 188-189 °C

| | | | | |
|---|---|---|---|---|
| **ESI-HRMS** ($[C_{38}H_{32}N_4O_2]^+$): | measured: | 530.2326 | | |
| | calculated: | 530.2339 | | |
| **Elemental analysis:** ($C_{38}H_{32}N_4O_2 \cdot H_2O$) | calculated: | %C 79.0 | %H 5.4 | %N 12.8 |
| | found: | %C 79.8 | %H 5.8 | %N 12.2 |

### 1.1.7 UV/Vis spectra of $L^{Et}$, $L^{tBu}$, $L^{Ph}$ and $L^{CN}$

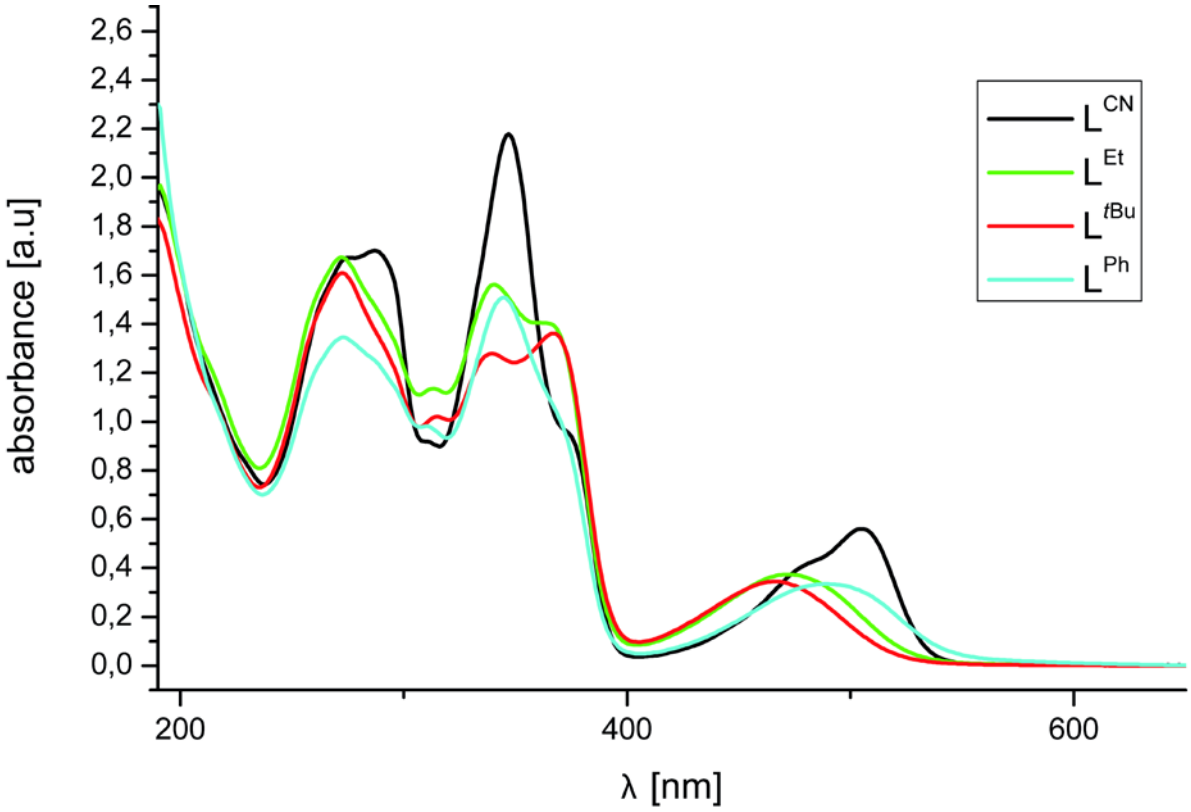


Fig. SI1 - UV/Vis spectra of all ligands. The bathochromic shift from 466 nm for the ligand $L^{tBu}$ (red) to 489 nm for the $L^{Ph}$ (cyan) correlates with the observations made in the NMR experiments. The more pronounced the electron withdrawing character of the headgroup, the stronger the bathocromic shift and the higher the single bond character of the exocyclic C=C bond, leading to faster rotation. This is effect is in accordance with literature described systems.[2]

### 1.1.8 2-cyano-2-(10-hexyl-9-acridinylidene)ethylacetate (15)

$TiCl_4$ (255 mg, 1.34 mmol, 1.25 equiv.) was slowly added to **14** (300 mg, 1.07 mmol, 1.00 equiv.) solved in dry $CH_2Cl_2$ (15 mL) and stirred for 15min at room temperature. 2-cyanoethylacetate (243 mg, 2.15 mmol, 2.00 equiv.) and triethylamine (2 mL) were added consecutively to the reaction mixture and heated to 70°C under reflux for 24 h. The cooled down reaction mixture was filtered through celite and the residue was washed with $CH_2Cl_2$ (2 x 50mL). The solvent was removed *in vacuo* and the residue was purified by means of column chromatography ($SiO_2$, chloroform/methanol 40:1 → 20:1). The product (316 mg, 0.84 mmol, 79%) was obtained as an orange solid.

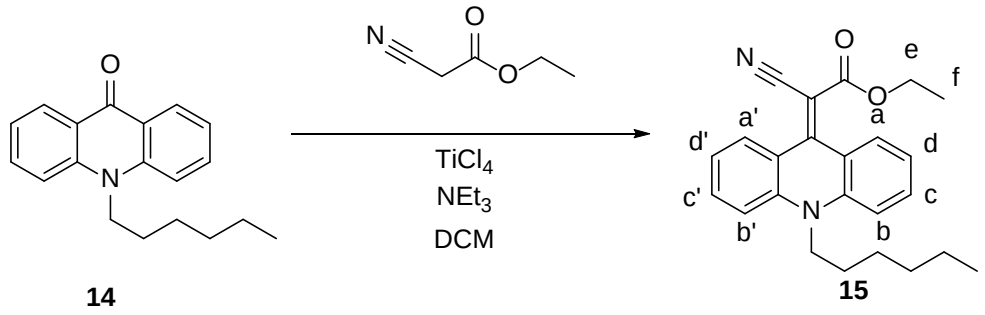


**14** **15**

**$^1$H-NMR** (300 MHz, 298 K, $CD_3CN$): $\delta$ (ppm) = 8.02 (d, $J$ = 8.1 Hz, 2H, a/a'), 7.62 (ddd, $J$ = 8.6, 7.0, 1.5 Hz, 2H, c/c'), 7.53 (dd, $J$ = 8.7, 0.7 Hz, 2H, b/b'), 7.20 (ddd, $J$ = 8.1, 7.0, 1.1 Hz, 2H, d/d'), 4.36 – 4.25 (m, 2H, NC**H$_2$**), 4,30 (q, $J$ = 7.1 Hz, 2H, OC**H$_2$**), 1.92 – 1.81 (m, 2H, $NCH_2C$**H$_2$**), 1.49 – 1.41 (m, 2H, $NCH_2CH_2C$**H$_2$**), 1.40 – 1.28 (m, 4H, C**H$_2$**C**H$_2$**$CH_3$), 1.17 (t, $J$ = 7.1 Hz, 3H, $OCH_2C$**H$_3$**). , 0.91 (t, $J$ = 7.1 Hz, 3H, $CH_2CH_2C$**H$_3$**).

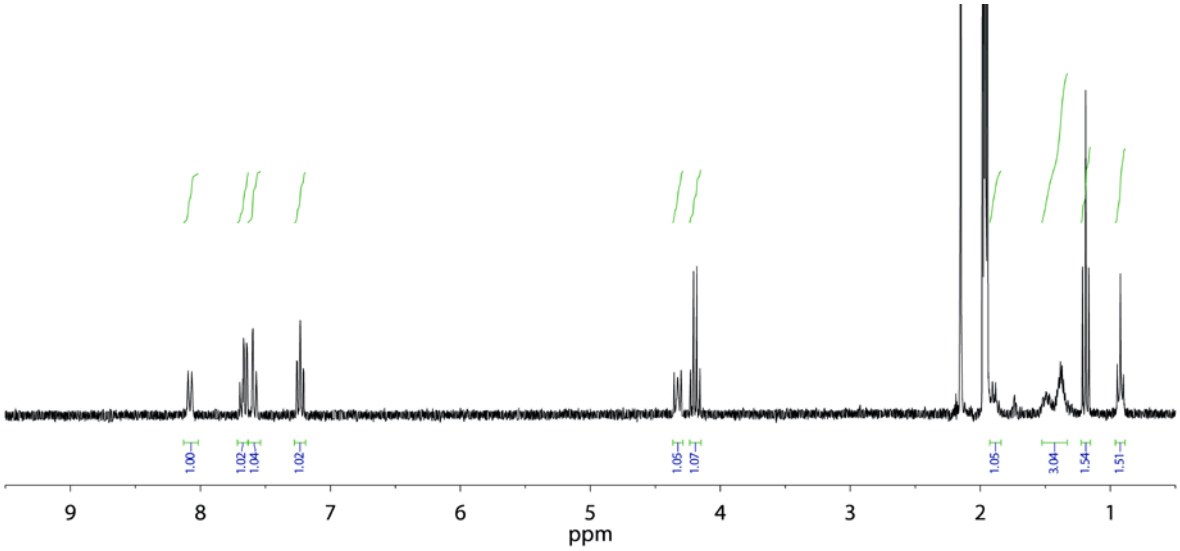

**$^{13}$C-NMR** (176 MHz, 298 K, $CD_3CN$): $\delta$ (ppm) = 166.2, 152.9, 140.1, 133.5, 128.8, 121.8, 120.3, 119.9, 118.3, 115.4, 91.9, 62.5, 48.0, 32.0, 27.2, 27.0, 23.3, 14.3, 14.2.

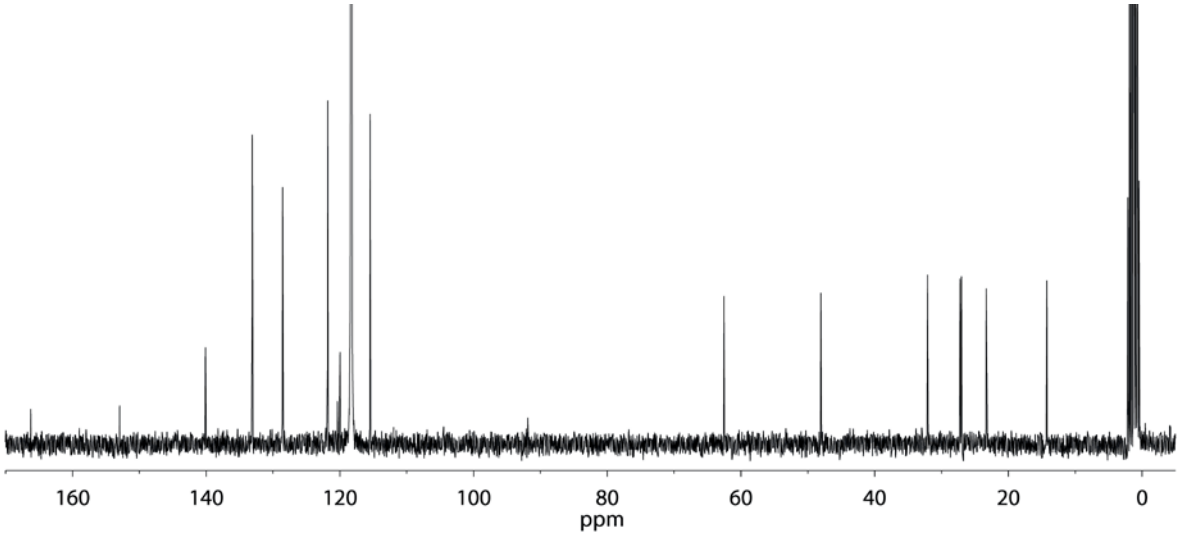


**UV/Vis (MeCN):** $\lambda_{max}$ ($\varepsilon$)=237 (40300), 290 (24900), 455 (17300).

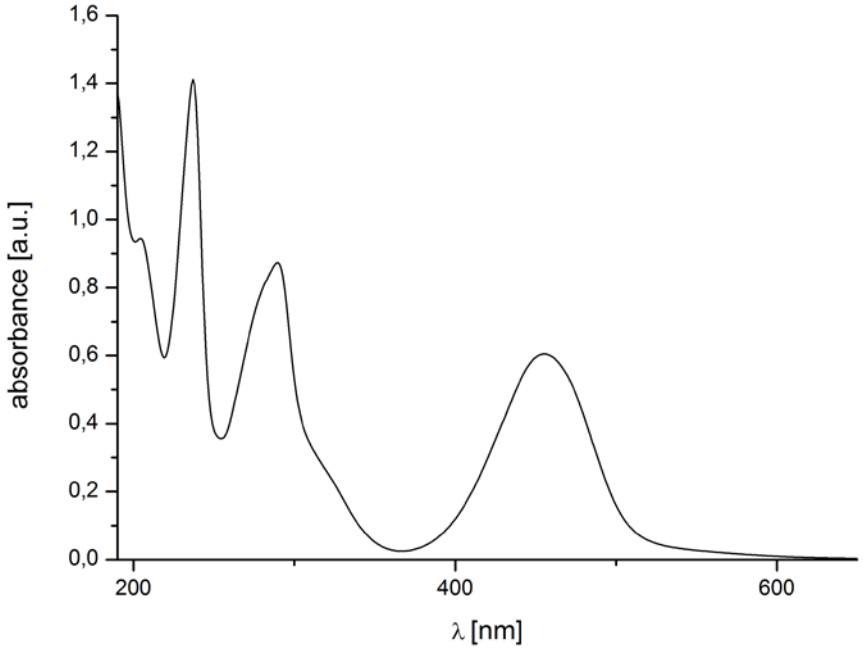


**IR (ATR):** $\tilde{\nu}$ ($cm^{-1}$) = 2924, 2868, 2193, 1709, 1601, 1577, 1507, 1460, 1377, 1263, 1231, 1103, 751, 659.

**Melting point:** 94-95 °C

**ESI-HRMS** ($[C_{38}H_{32}N_4O_2]^+$): measured: 375.2064

calculated: 375.2067

## 1.2 Cage Syntheses

### General Procedure

Ligand $\mathbf{L}^{R=Et,\ tBu,\ Ph}$ (500 µL, 2.8 mmol, 1.0 eq.), $[Pd_2(CH_3CN)4](BF_4)$ (50 µL, 15 mmol, 0.5 eq.) and were heated to 80 °C in deuterated acetonitrile over night. The $[Pd_2\mathbf{L}^R{}_4]$ cage was formed quantitatively as a 0.70 mM solution.

### 1.2.1 $[Pd_2L^{Et}{}_4](BF_4)_4$ (10)

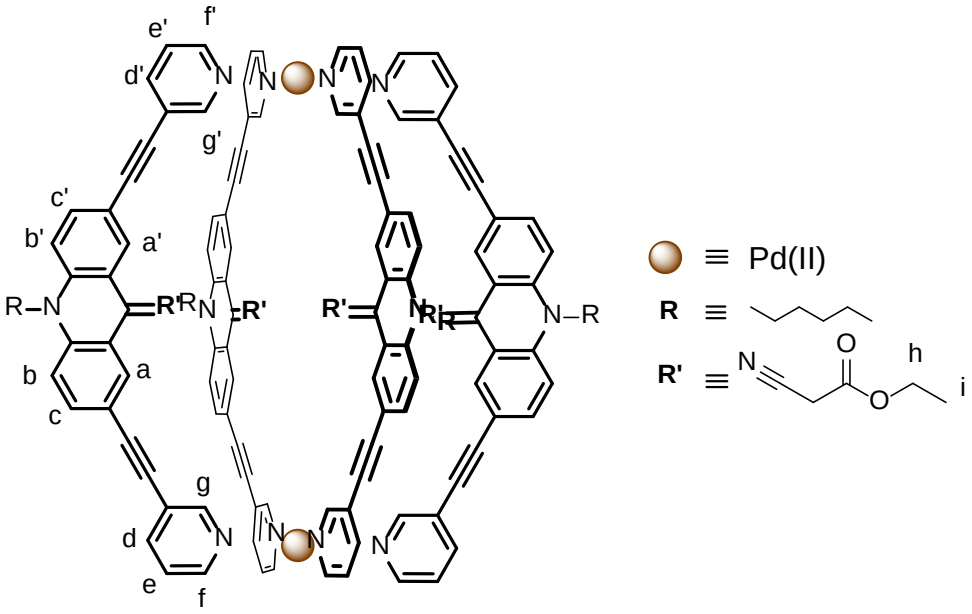


**$^1$H-NMR** (400 MHz, 298 K, $CD_3CN$): $\delta$ (ppm) = 9.19 (s, 2H, g/g'), 8.95 (dd, $^3J$ = 5.0, $^4J$ = 1.7 Hz, 2H, f/f'), 8.35 (s, 2H, a/a'), 8.10 (dt, $^3J$ = 7.9,$^4J$= 2.0 Hz, 2H, d/d'), 7.78 (dd, $^3J$ = 9.0, $^4J$= 2.0 Hz, 2H, c/c'), 7.63 (dt,$^3J$ = 7.9,$^4J$ = 4.8 Hz,2H, e/e*),7.57 (d, $^3J$ = 8.9 Hz, 2H, b/b'), 4.30 – 4.21 (m, 2H, NC$\underline{H}_2$), 4.00 (q, $^3J$ = 7.2 Hz, 2H, h), 1.86 – 1.77 (m, 2H, C$\underline{H}_2$), 1.45 – 1.37(m, 2H, C$\underline{H}_2$), 1.36 – 1.23(m, 4H, C$\underline{H}_2$C$\underline{H}_2$CH$_3$), 0.87 (t, $^3J$ = 7.1 Hz, 3H, i) 0.83 (t, $^3J$ = 7.0 Hz, 3H, C$\underline{H}_3$).

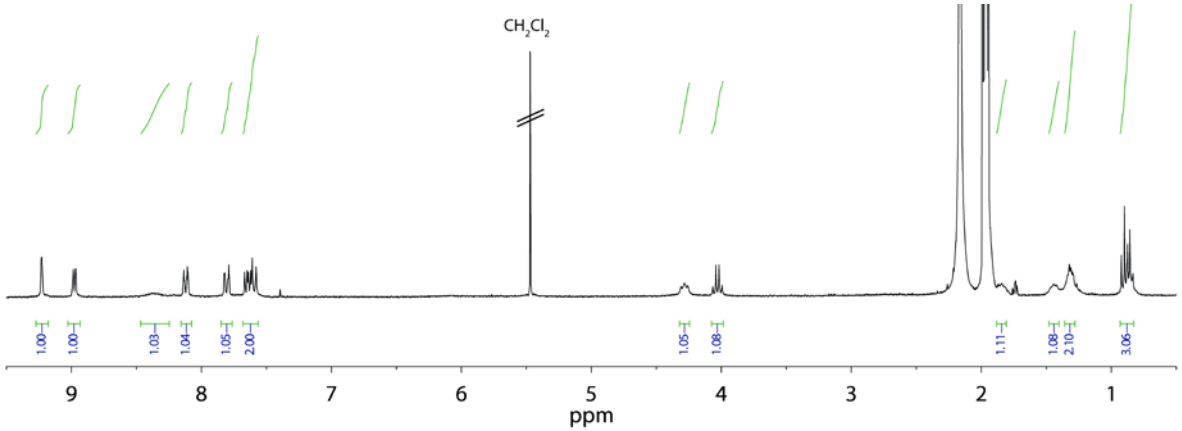


**ESI-HRMS** ($[C_{152}H_{128}N_{16}O_8Pd_2]^{4+}$: measured: 628.2029

calculated: 628.2046

### 1.2.2 $[Pd_2L^{tBu}{}_4](BF_4)_4$ (11)

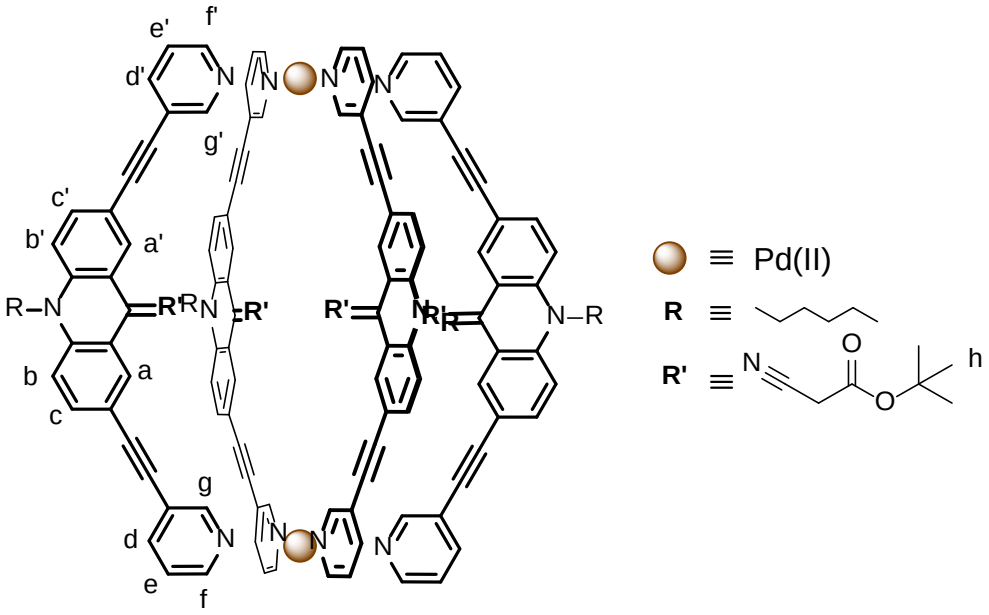


**$^1$H-NMR** (400 MHz, 298 K, $CD_3CN$): $\delta$ (ppm) = 9.17 (s, 2H, g/g'), 8.94 (dd, $^3J$ = 5.0, $^4J$ = 1.7 Hz, 2H, f/f'), 8.09 (dt, $^3J$ = 7.9,$^4J$= 2.0 Hz, 2H, d/d'), 7.79 (dd, $^3J$ = 9.0, $^4J$= 2.0 Hz, 2H, c/c'), 7.63 (dt,$^3J$ = 7.9,$^4J$ = 4.8 Hz,2H, e/e*), 7.56 (d, $^3J$ = 8.9 Hz, 2H, b/b'), 4.32 – 4.13 (m, 2H, $NCH_2$), 1.88 – 1.74 (m, 2H, $CH_2$), 1.42 – 1.28 (m, 2H, $CH_2$), 1.31 – 1.18 (m, 4H, $CH_2CH_2CH_3$), 1.01 (s, 9H, h), 0.92 (t, $J$ = 7.0 Hz, 3H, $CH_3$).

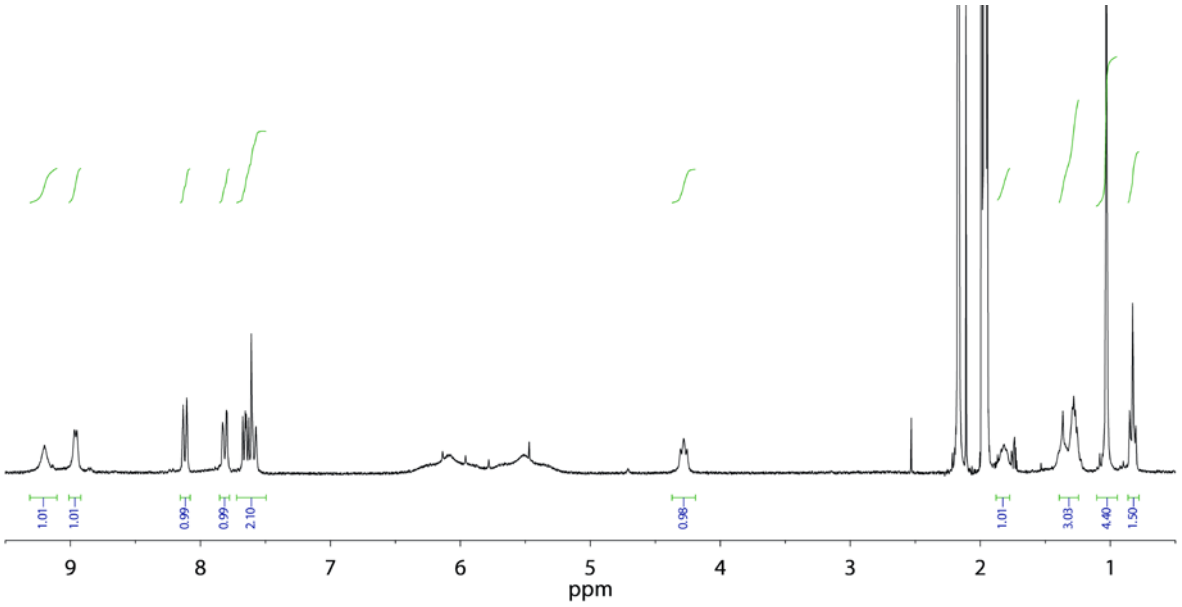


**ESI-HRMS** ($[C_{160}H_{144}N_{16}O_8Pd_2]^{4+}$: measured: 656.2363

calculated: 656.2359

### 1.2.3 $[Pd_2L^{Ph}_4](BF_4)_4$ (12)

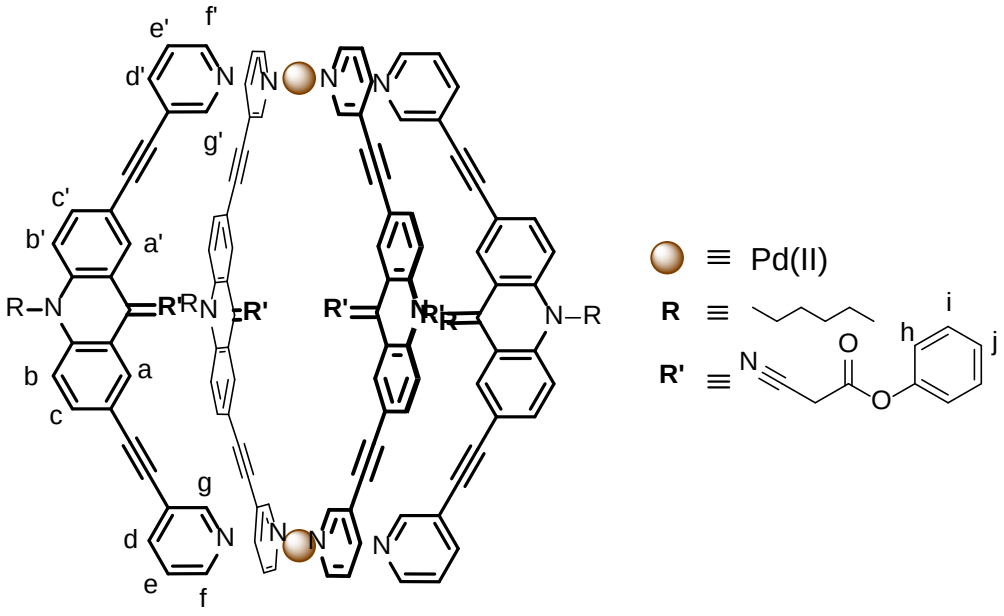


**$^1$H-NMR** (400 MHz, 298 K, $CD_3CN$): $\delta$ (ppm) = 9.18 (s, 2H, g/g'), 9.01 (dd, $^3J$ = 5.0, $^4J$ = 1.7 Hz, 2H, f/f'), 8.37 (d, $^4J$ = 2.0 Hz, 2H, a/a'), 8.11 (dt, $^3J$ = 7.9,$^4J$= 2.0 Hz, 2H, d/d'), 7.71 (dd, $^3J$ = 9.0, $^4J$= 2.0 Hz, 2H, c/c'), 7.65 (dt,$^3J$ = 7.9,$^4J$ = 4.8 Hz,2H, e/e*), 7.55 (d, $^3J$ = 8.9 Hz, 2H, b/b'), 7.08 – 6.97 (m, 3H, h,j), 6.86 – 6.80 (m, 2H, i), 4.35 – 4.16(m, 2H, $NCH_2$), 1.84 – 1.66(m, 2H, $CH_2$), 1.45 – 1.31 (m, 2H, $CH_2$), 1.31 – 1.19 (m, 4H, $CH_2CH_2CH_3$), 0.83 (t, $^3J$ = 7.0 Hz, 3H, $CH_3$).

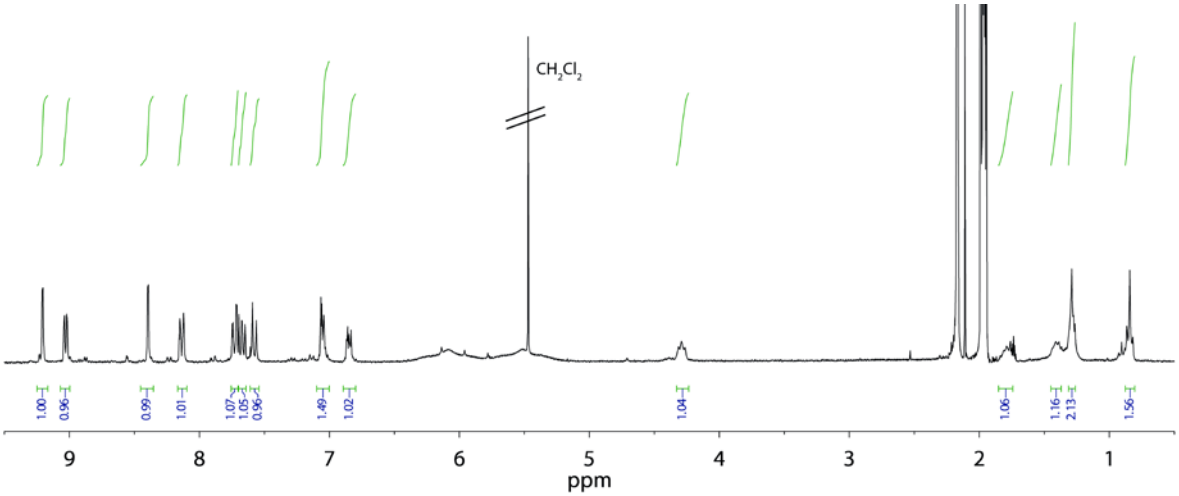


**ESI-HRMS** ($[C_{168}H_{128}N_{16}O_8Pd_2]^{4+}$: measured: 676.4550

calculated: 676.4547

### 1.2.4 $[Pd_2L^{CN}_4](BF_4)_4$ (13)

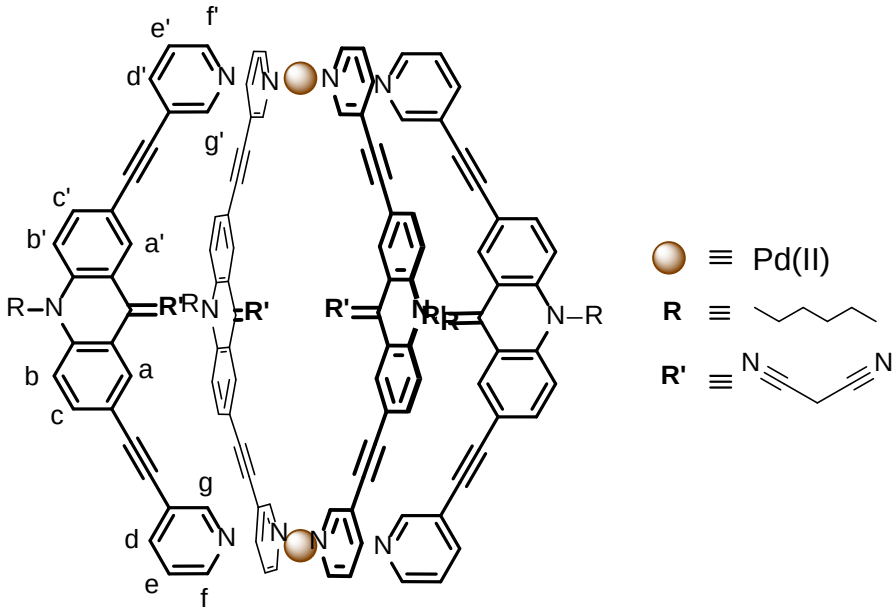


**$^1$H-NMR** (400 MHz, 298 K, $CD_3CN$): $\delta$ (ppm) = 9.32 (dd, $^4J$ = 2.2 Hz, 2H, g), 9.02 (dd, $^3J$ = 4.9, $^4J$ = 1.7 Hz, 2H, f), 8.80 (d, $^4J$ = 1.9 Hz, 2H, a), 8.09 (dt, $^3J$ = 7.9,$^4J$= 2.0 Hz, 2H, d), 7.89 (dd, $^3J$ = 3.7, $^4J$ = 1.9 Hz, 2H, c), 7.71 (d, $^3J$ = 9.1 Hz, 2H, b), 7.62 (dd, $^3J$ = 7.9, $^4J$ = 4.9, 2H, e), 4.47 – 4.24 (m, 2H, $NC\underline{H}_2$), 1.92 – 1.78 (m, 2H, $C\underline{H}_2$) 1.51 – 1.40 (m, 2H, $C\underline{H}_2$), 1.37 – 1.24 (m, 4H, $C\underline{H}_2C\underline{H}_2CH_3$), ), 0.84 (t, $J$ = 7.0 Hz, 3H, $C\underline{H}_3$).

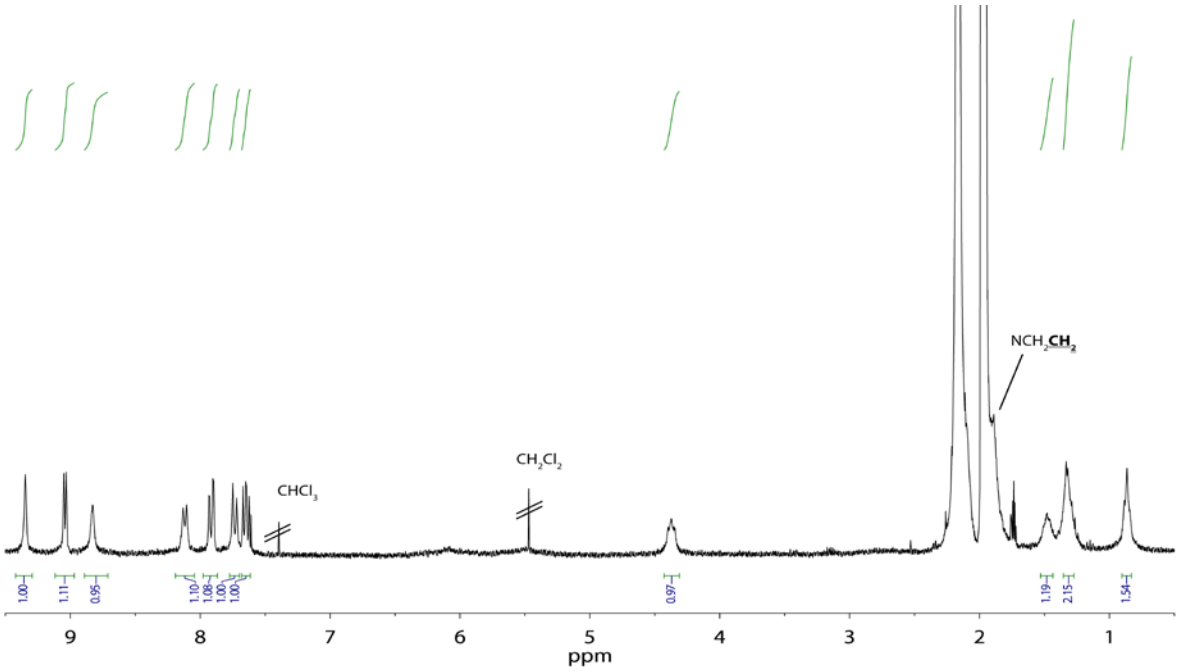


**ESI-HRMS** ($[C_{168}H_{128}N_{16}O_8Pd_2]^{4+}$: measured: 581.4256

calculated: 581.4287

### 1.2.5 ESI-MS spectra of $[Pd_2L^{Et}_4](BF_4)_4$, $[Pd_2L^{tBu}_4](BF_4)_4$ and $[Pd_2L^{Ph}_4](BF_4)_4$

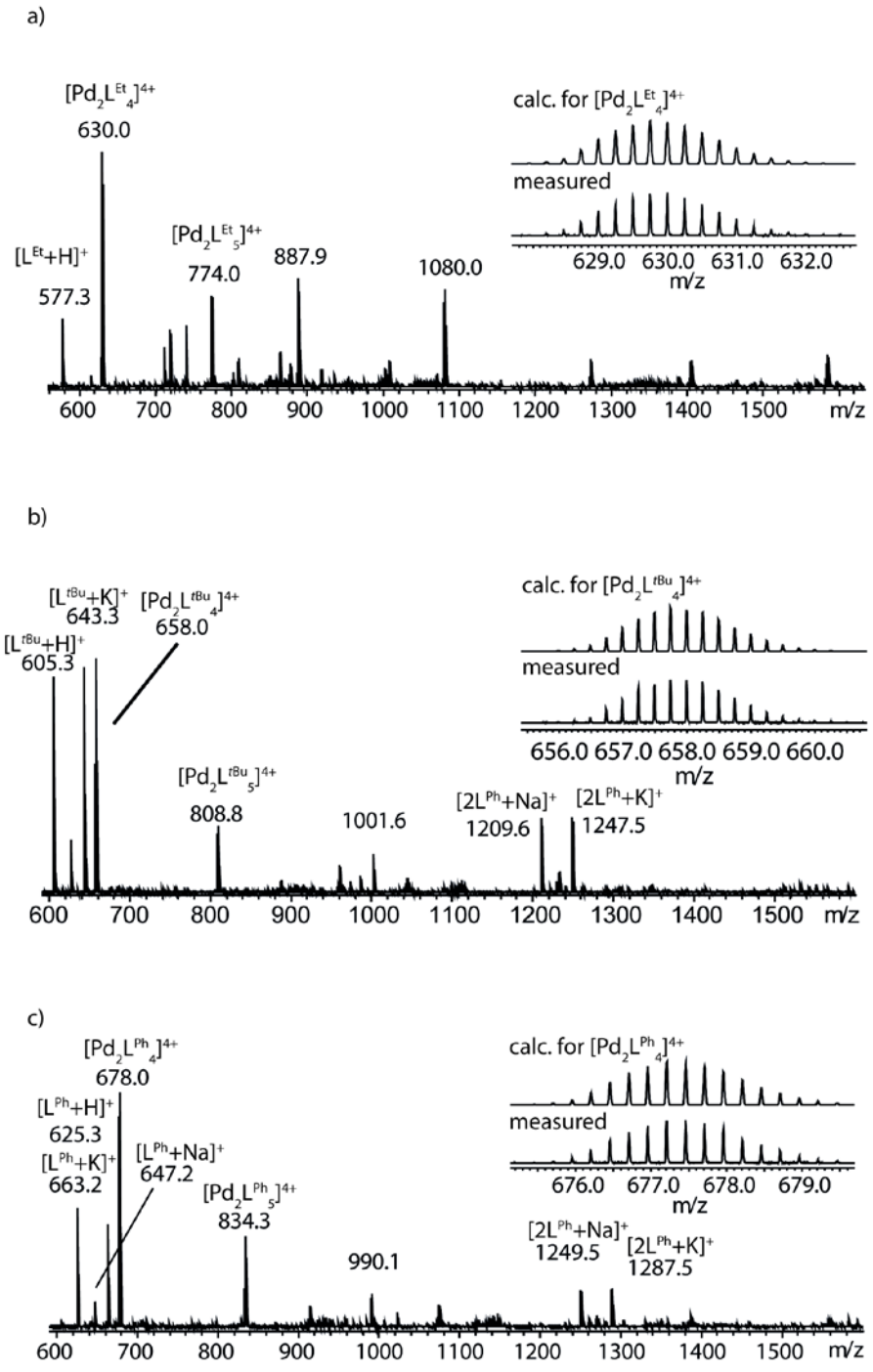


**Figure SI1** ESI-MS of cages (a) $[Pd_2\mathbf{L}^{Et}_4]$ (b) $[Pd_2\mathbf{L}^{tBu}_4]$ and (c) $[Pd_2\mathbf{L}^{Ph}_4]$.

### 1.2.6 Solvent effect on the NMR chemical shifts of ligand $L^{Et}$ and the $[Pd_2L^{Et}_4]$ cage

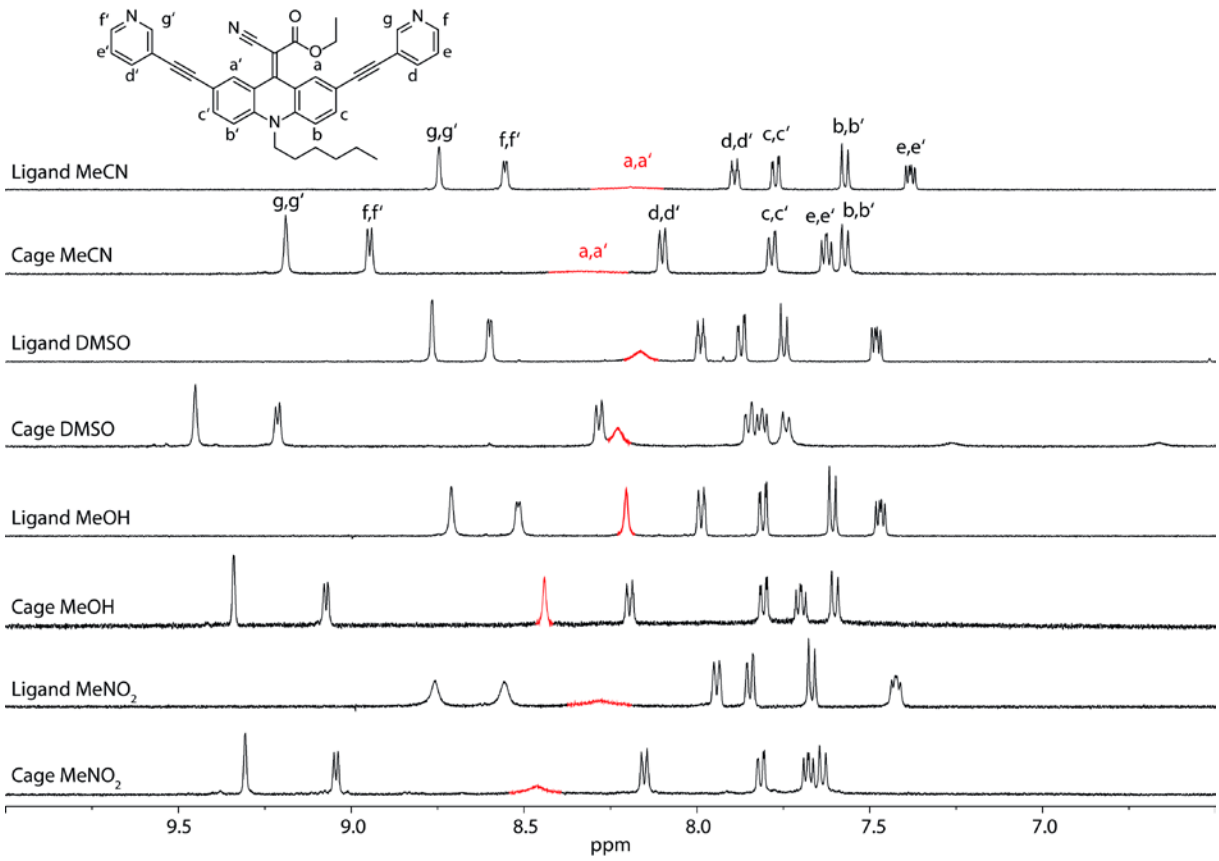


**Figure SI2** $^1$H NMR spectra (400 MHz, 298 K) of ligand $\mathbf{L^{Et}}$ and cage $[Pd_2\mathbf{L^{Et}}_4]$ in different solvents. The spinning rate of the rotor groups and the associated sharpness of the signal a/a' (red) depends on the polarity of the solvent with the rotational rate rising in the order MeCN>$MeNO_2$>dmso>MeOH. In all cases, the sharpness of the a/a' signal increases upon cage formation.

# 2 Variable Temperature NMR Experiments of ligands

## 2.1 VT-NMR of $L^{Et}$

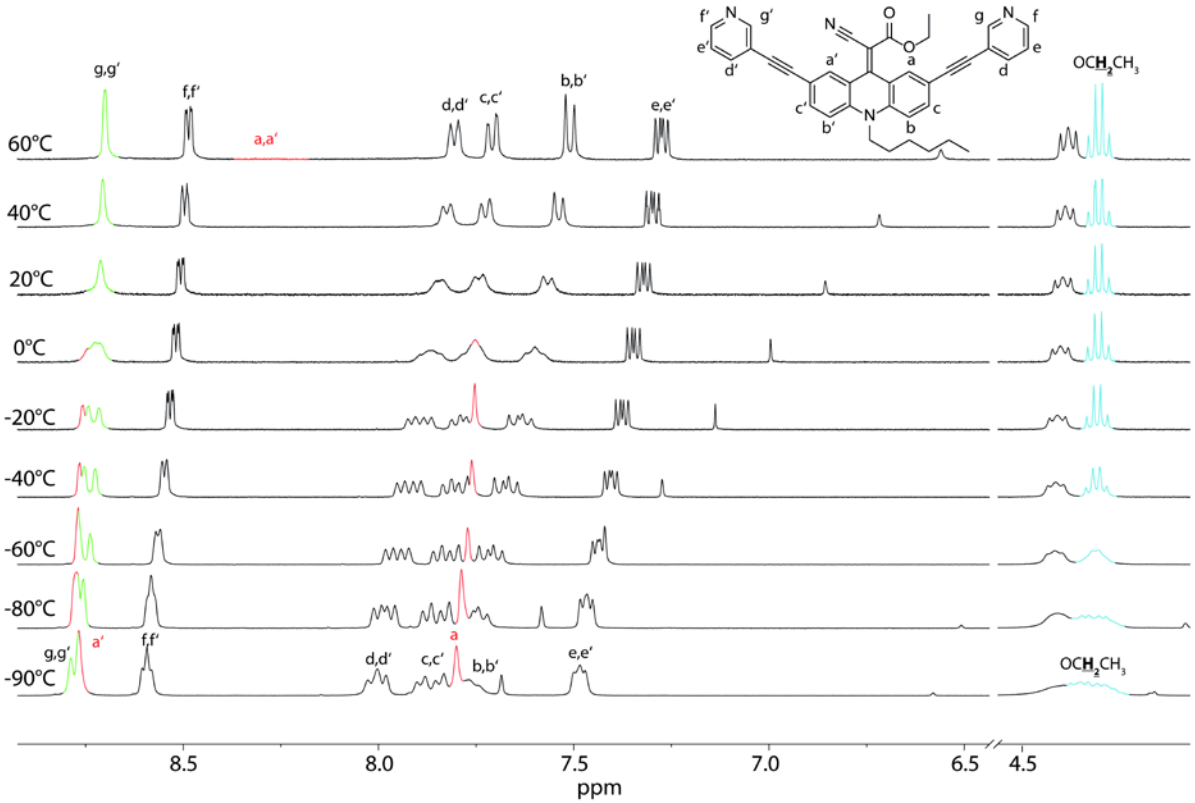


**Figure SI3** VT $^{1}$H NMR spectra (400 MHz, $d^{8}$-THF) of ligand $\mathbf{L^{Et}}$. The rotation rate and the associated signal sharpness of a/a' (red) depend on the temperature. At low temperatures two sets of signals are observable due to the low rotation rate. Higher temperatures lead to increased rotation rates and one set of signals. The coalescence temperature is around 40°C. The $CH_2$-group of the ethyl group seems to split into to quartets at very low temperatures. This is an indication for a flipping motion of the backbone (compare Fig. SI6).

## 2.2 VT-NMR of $L^{tBu}$

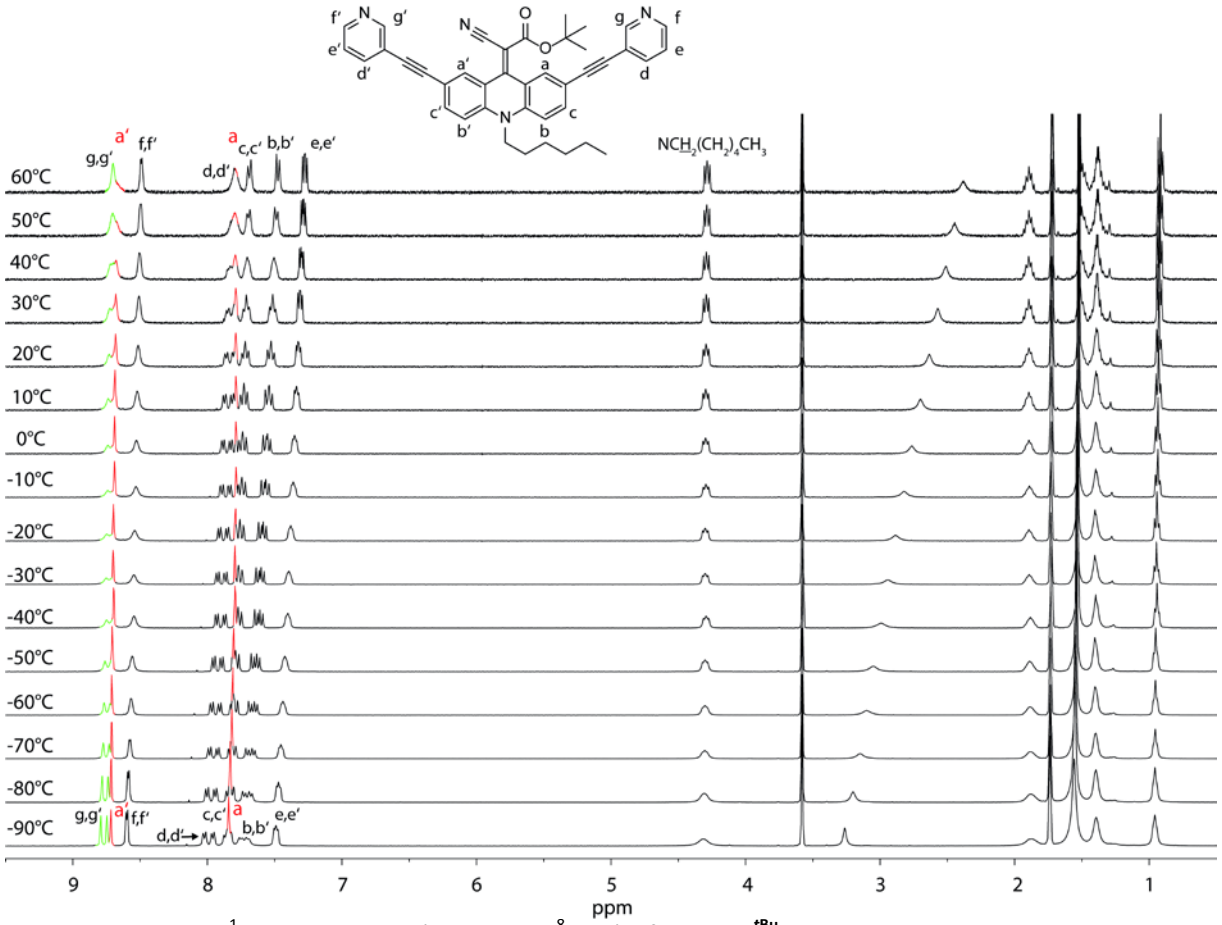


**Figure SI4** VT $^{1}$H NMR spectra (400 MHz, $d^{8}$-THF) of ligand $\mathbf{L^{tBu}}$. The rotation rate and the associated signal sharpness of a/a' (red) depend on the temperature. At low temperature two sets of signals are observable due to a low rotation rate. Higher temperatures increase the rotation rates and lead to one set of signals. The coalescence temperature is not reached in this experiment.

## 2.3 VT-NMR of $L^{Ph}$

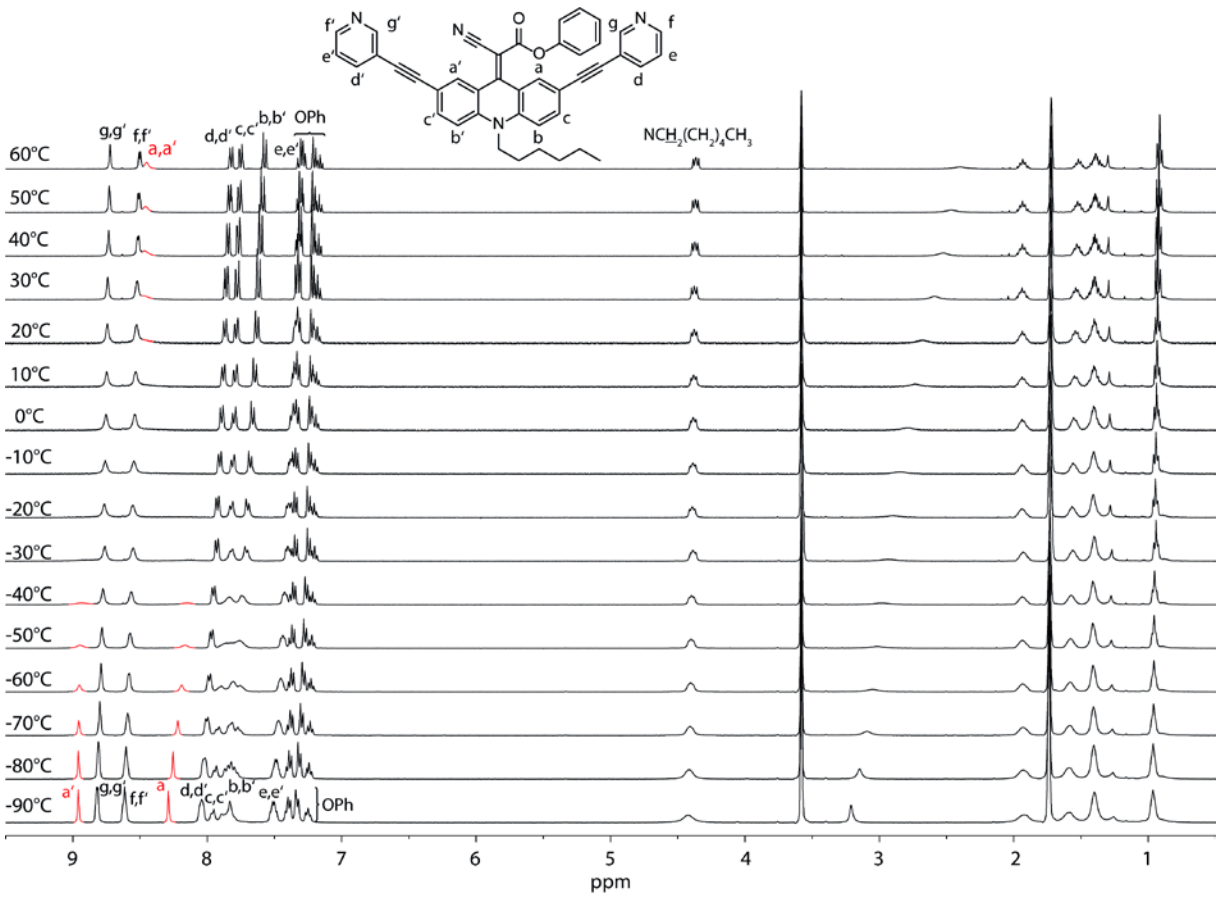


**Figure SI5** VT $^{1}$H NMR spectra (400 MHz, $d^{8}$-THF) of ligand $\mathbf{L^{Ph}}$. The rotation rate and the associated signal sharpness of a/a' (red) depend on the temperature. At low temperature two sets of signals are observable due to a low rotation rate. Higher temperatures increase the rotation rate and lead to one set of signals. The coalescence temperature is around -10°C

## 2.4 Comparison VT-NMR of Ligand $L^{Et}$ and Backbone $B^{Et}$

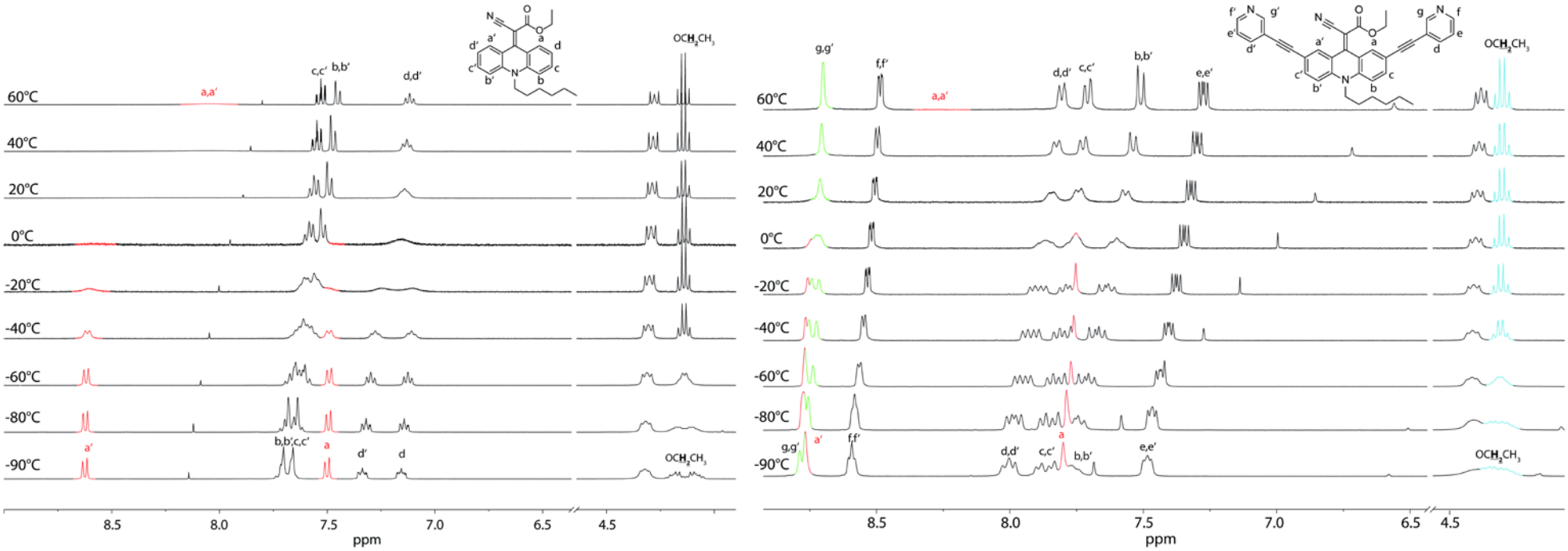


**Figure SI6** Comparison of VT $^{1}$H NMR spectra (400 MHz, d$^{8}$-THF) of backbone $\mathbf{B^{Et}}$ and ligand $\mathbf{L^{Et}}$. Both compounds show a similar behavior of rotation towards variation of temperature. Furthermore, in both cases coalescence temperature is reached around 30°C and the splitting of ethyl group protons is observable at low temperatures.

## 2.5 VT-NMR of $B^{Et}$

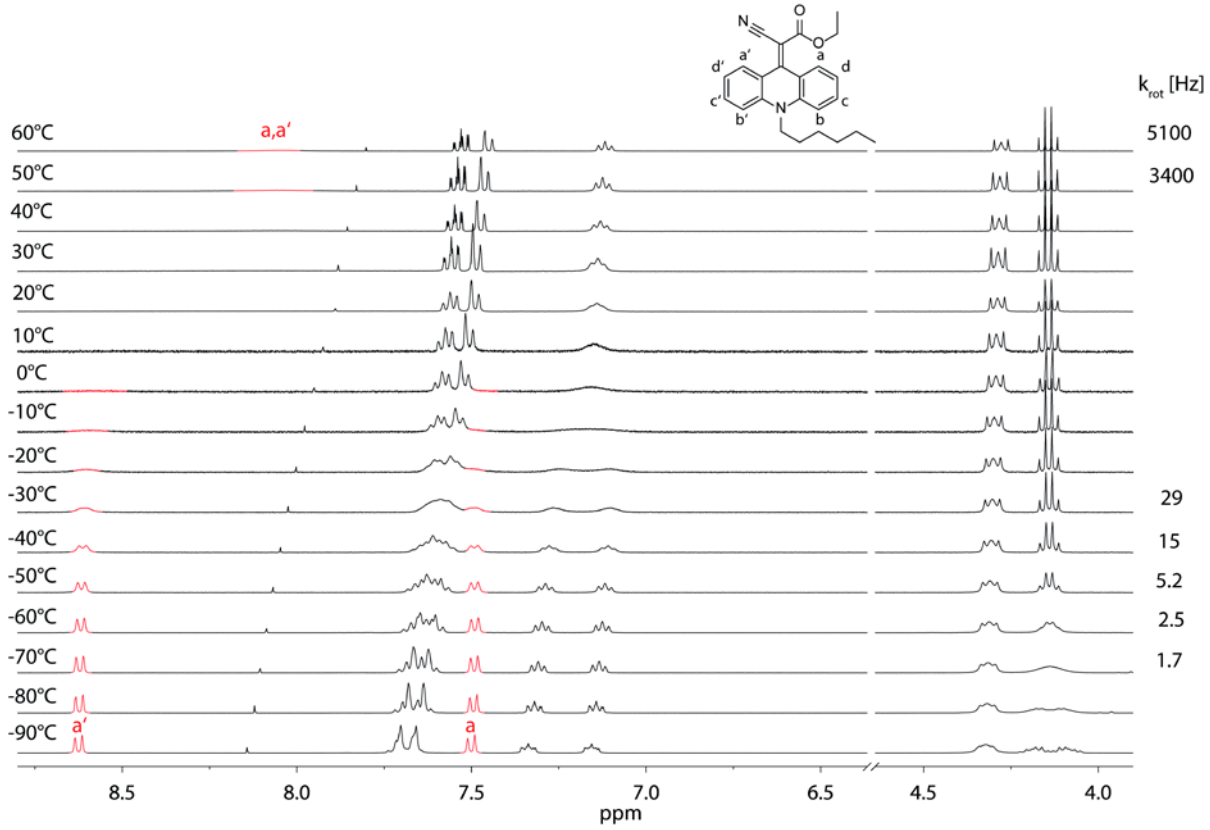


**Figure SI7** VT $^{1}$H NMR spectra (400 MHz, $d^{8}$-THF) of backbone $\mathbf{B^{Et}}$. Rotation rates at different temperatures were calculated by full lineshape analysis. At low temperature two sets of signals are observable due to low rotation rate. Higher temperatures increase rotation rate and lead to one set of signals. Coalescence temperature is reached around 30°C.

### 2.6.1 VT-NMR vs. DNMR3 Simulation of a/a' signals in $B^{Et}$

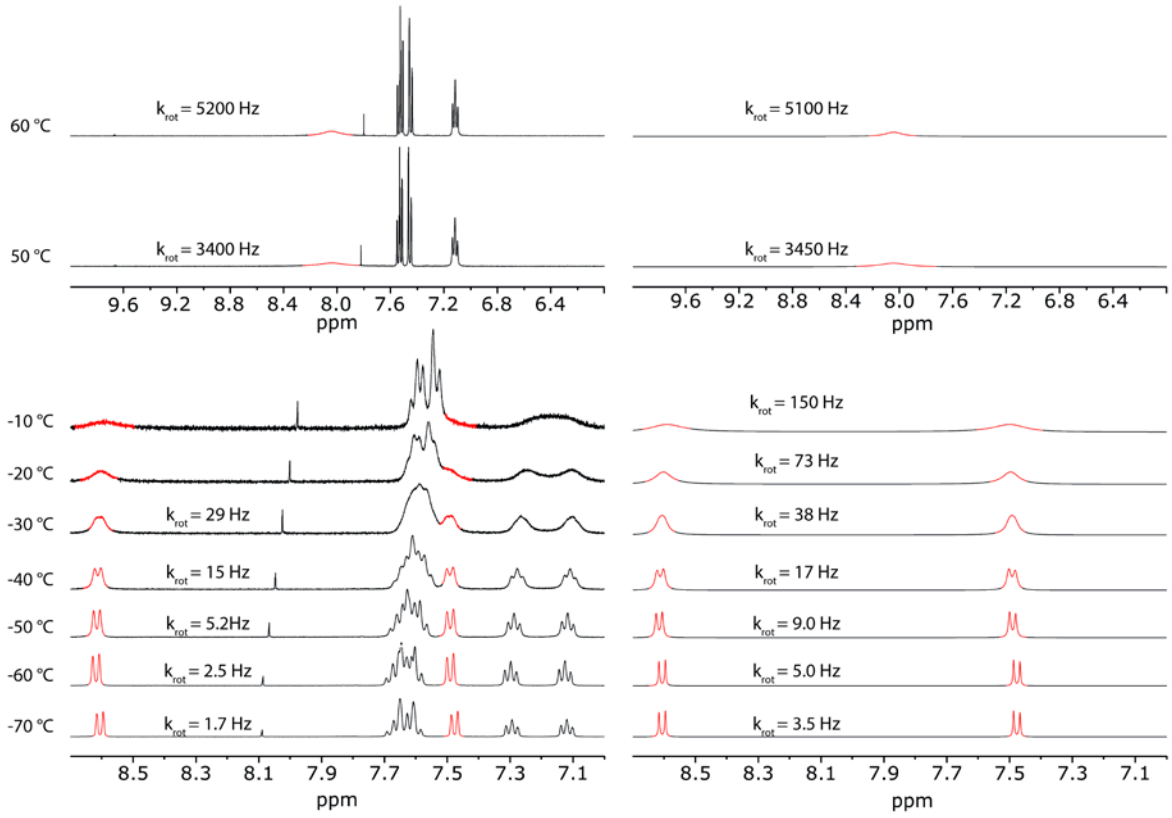


**Figure SI8** Rotation constants were extracted from (left) VT $^{1}$H-NMR experiments by full line shape analysis[3] and also by DNMR simulations (right) with the programm SpinWorks.[4]

### 2.6.2 Eyring plot of rotation constants extracted from VT $^{1}$H-NMR experiments

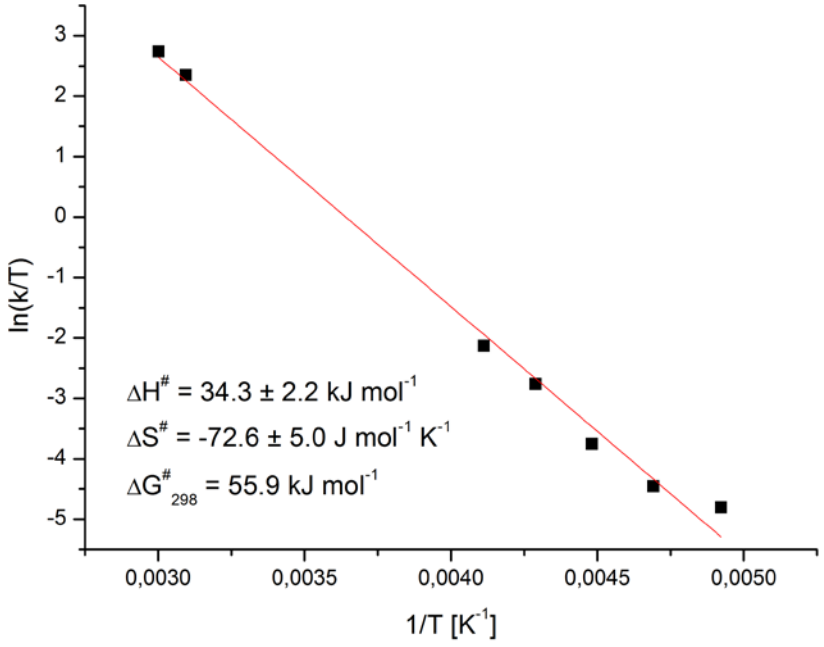


**Figure SI9** Energy barrier for the rotation motion in $\mathbf{B^{Et}}$ was calculated from plot ln(k/T) vs. $T^{-1}$. Rotation rates at different temperatures were extracted from VT $^{1}$H-NMR experiments (Fig. SI8) via full lineshape analysis.#

### 2.6.3 Eyring plot of rotation constants extracted from DNMR simulations

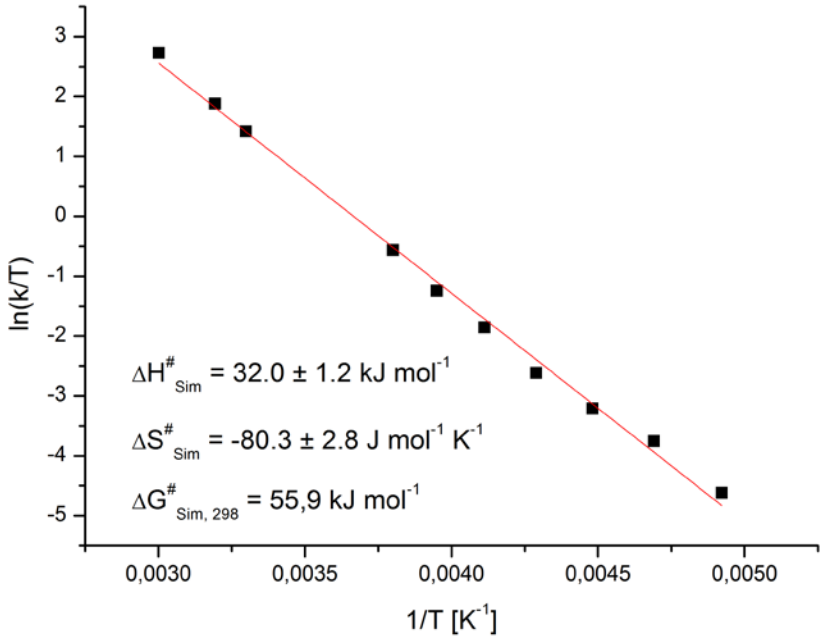


**Figure SI10** Activation enthalpy and entropy for the rotation motion in $\mathbf{B^{Et}}$ were calculated from Eyring plot ln(k/T) vs. $T^{-1}$. Rotation rates at different temperatures were taken from DNMR3 simulations (Fig. SI8), made with SpinWorks 4.2.4.

## 2.5 Rotation and flipping in ligand and cage

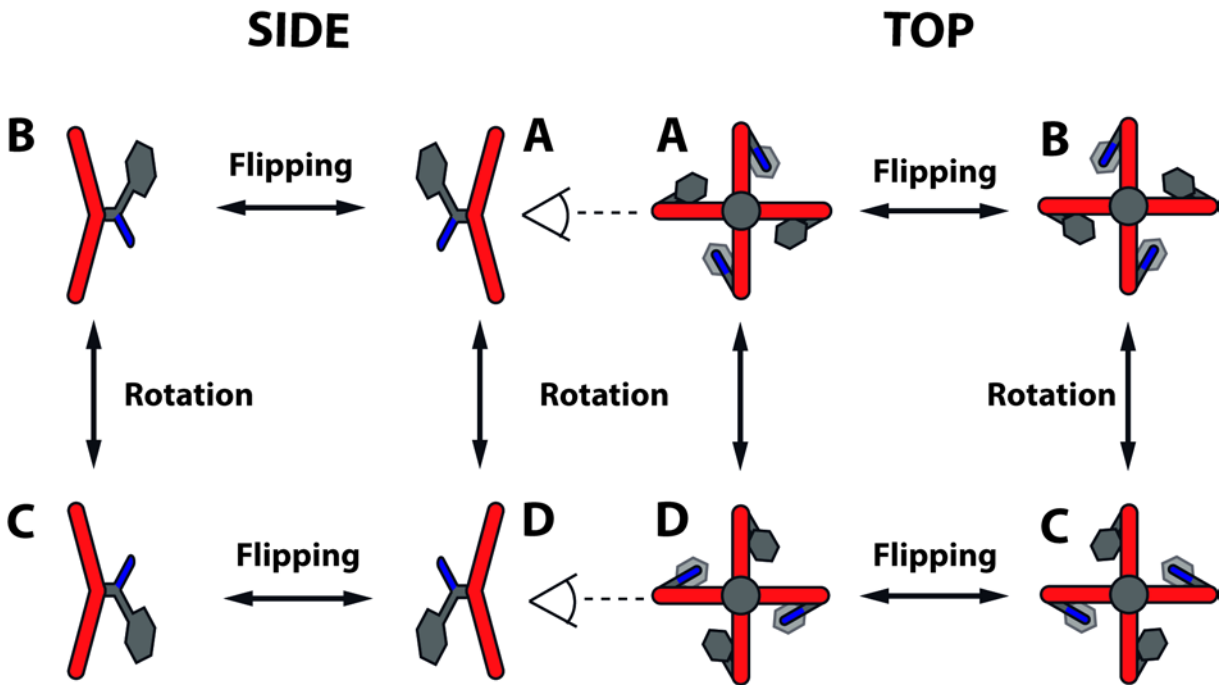


**Figure SI11** Scheme of flipping and rotating motions in the ligand and the [$Pd_2\mathbf{L}^{\mathbf{R}}_4$] cage. Comparable to our previously reported system that carries bulky adamantylidene substituents at the endohedral carbon position[5] we do not expect concerted flipping or rotation motions of the four ligands inside the cage.

# 3 Guest Titration NMR Experiments

## 3.1 Titration of $[Pd_2L^{Et}_4]$ cage with bis-anionic guests

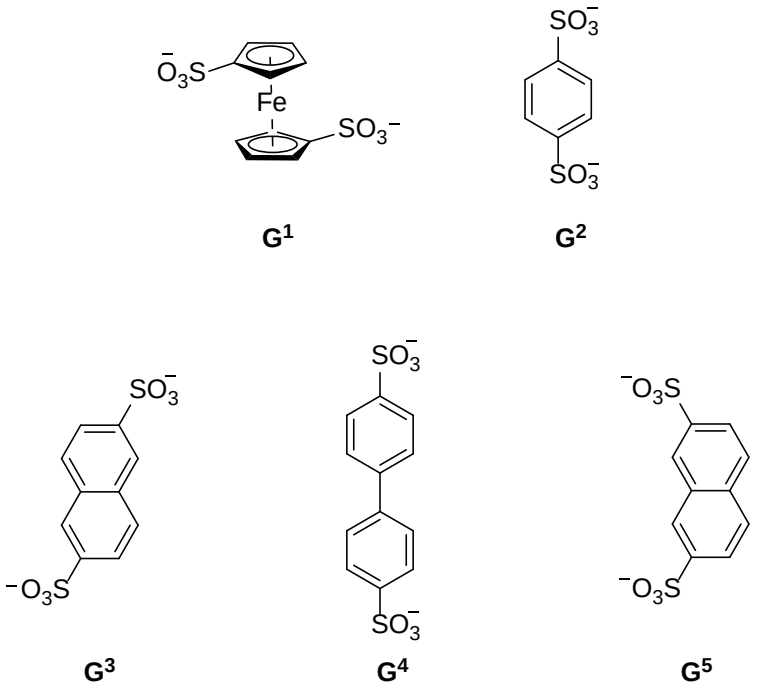


**G1** **G2** **G3** **G4** **G5**

**Figure SI12** Guest molecules $G^1$-$G^5$ for $^1$H-NMR host-guest titration experiments. All guests come with two tetra-n-butylammonium cations $(nBu)_4N^+$ counter-ions.

### 3.1.1 Titration of $[Pd_2L^{Et}_4]$ cage with $G^1$

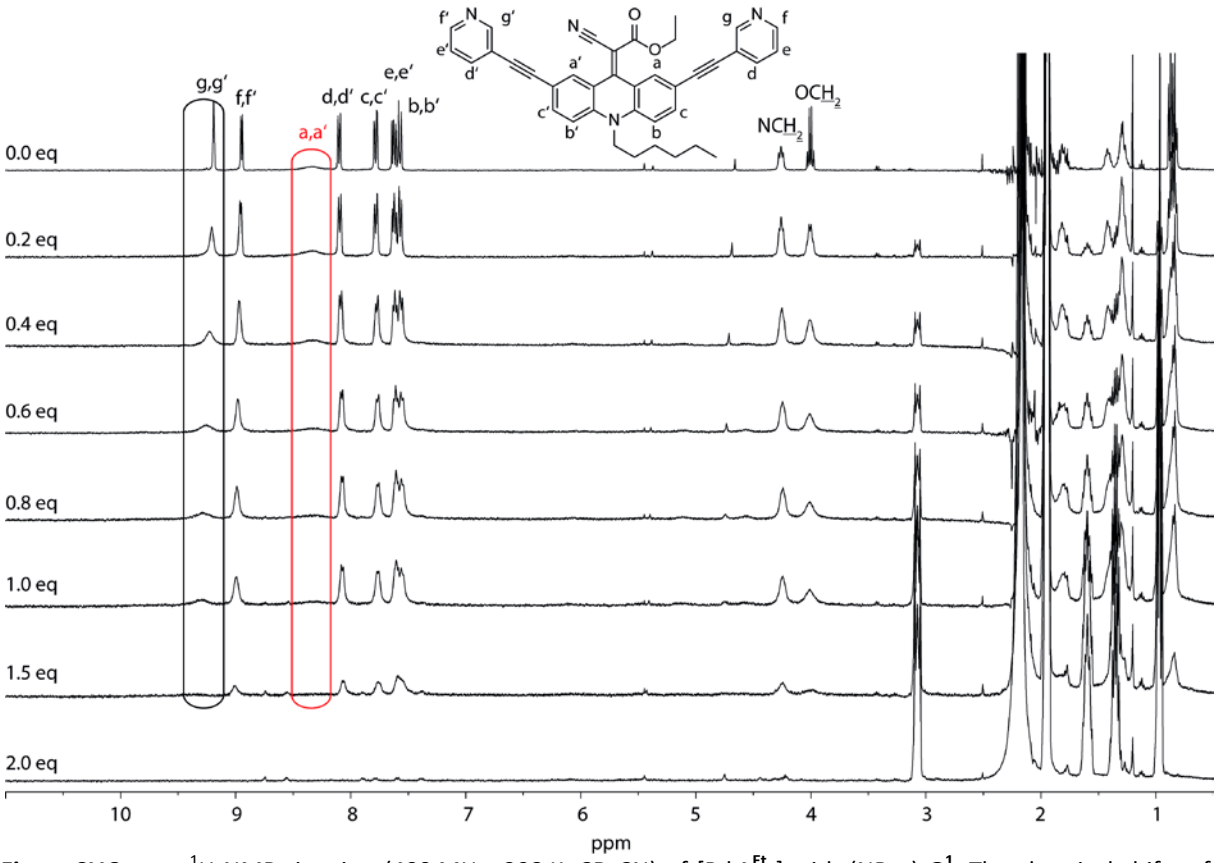


**Figure SI13** $^1$H NMR titration (400 MHz, 298 K, $CD_3CN$) of $[Pd_2\mathbf{L}^{\mathbf{Et}}_4]$ with $(NBu_4)_2\mathbf{G}^{\mathbf{1}}$. The chemical shifts of the inward pointing protons change gradually due to a fast exchange of the guest on the NMR time scale. Excess addition of $\mathbf{G}^{\mathbf{1}}$ leads to precipitation of the cage.

### 3.1.2 Titration of $[Pd_2L^{Et}_4]$ cage with $G^2$

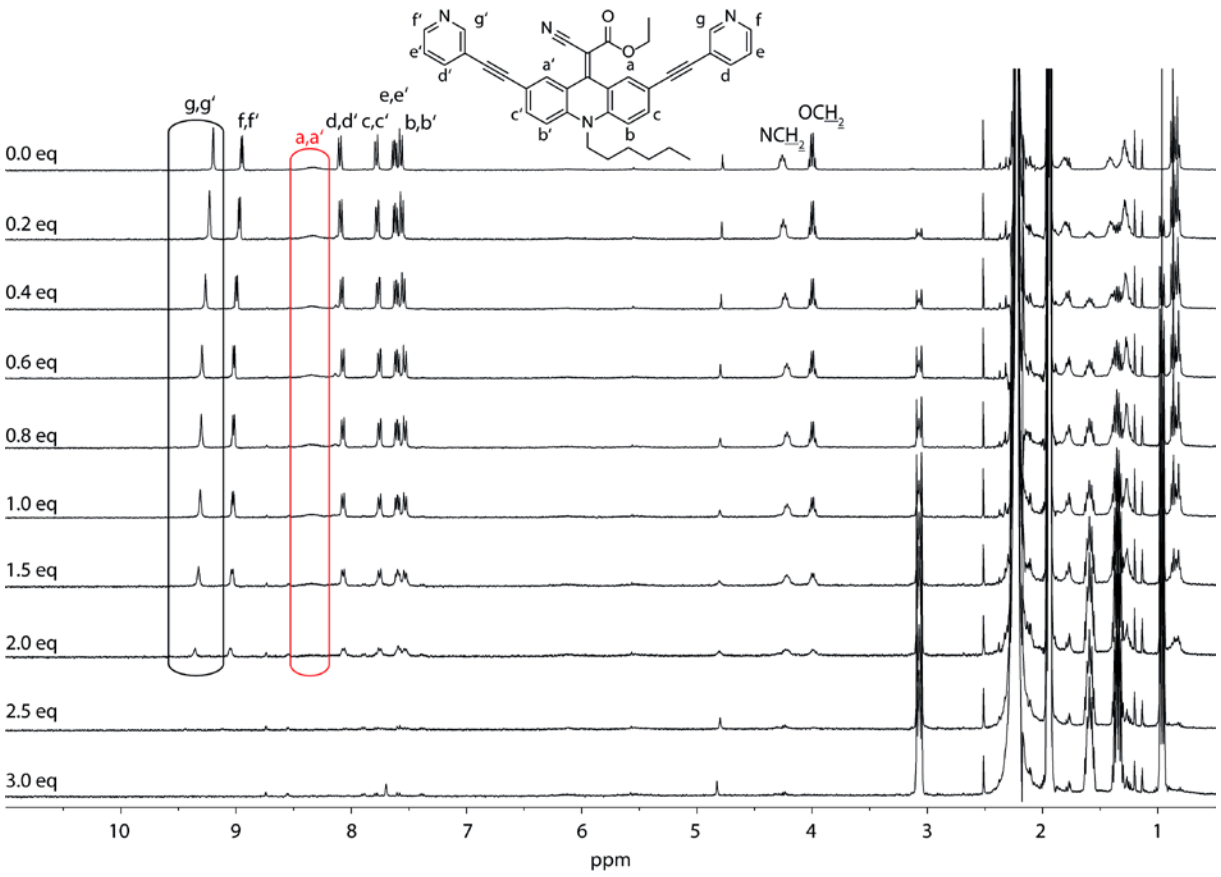


**Figure SI14** $^1$H NMR titration (400 MHz, 298 K, $CD_3CN$) of $[Pd_2L^{Et}_4]$ with $(NBu_4)_2G^2$. The chemical shifts of the inward pointing protons change gradually due to a fast exchange of the guest on the NMR time scale. Excess addition of $G^2$ leads to precipitation of the cage.

### 3.1.3 Titration of $[Pd_2L^{Et}_4]$ cage with $G^3$

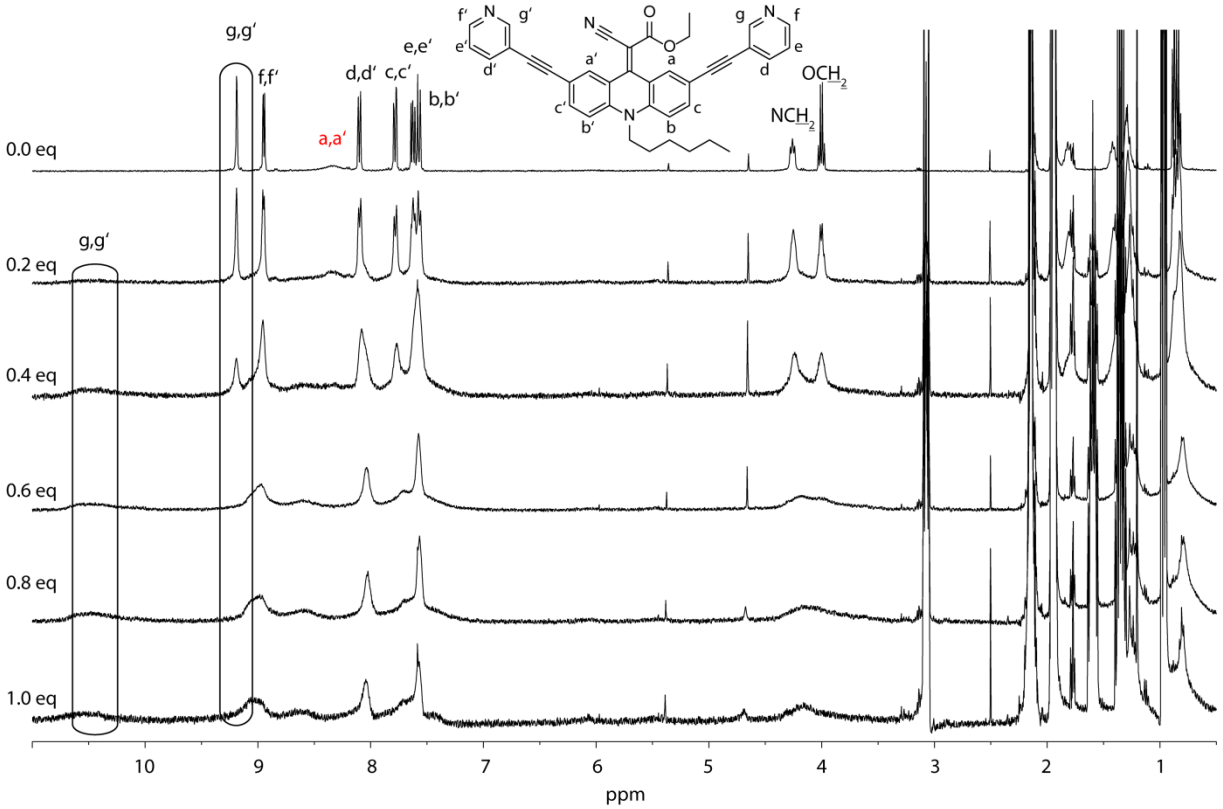


**Figure SI15** $^1$H NMR titration (400 MHz, 298 K, $CD_3CN$) of $[Pd_2\mathbf{L}^{Et}_4]$ with $(NBu_4)_2\mathbf{G}^3$. Upon addition of one equivalent of guest $\mathbf{G}^3$ the $[Pd_2\mathbf{L}^{Et}_4]$ cage transforms into $[\mathbf{G}^3@Pd_2\mathbf{L}^{Et}_4]$.

### 3.1.4 Titration of $[Pd_2L^{Et}_4]$ cage with $G_4$

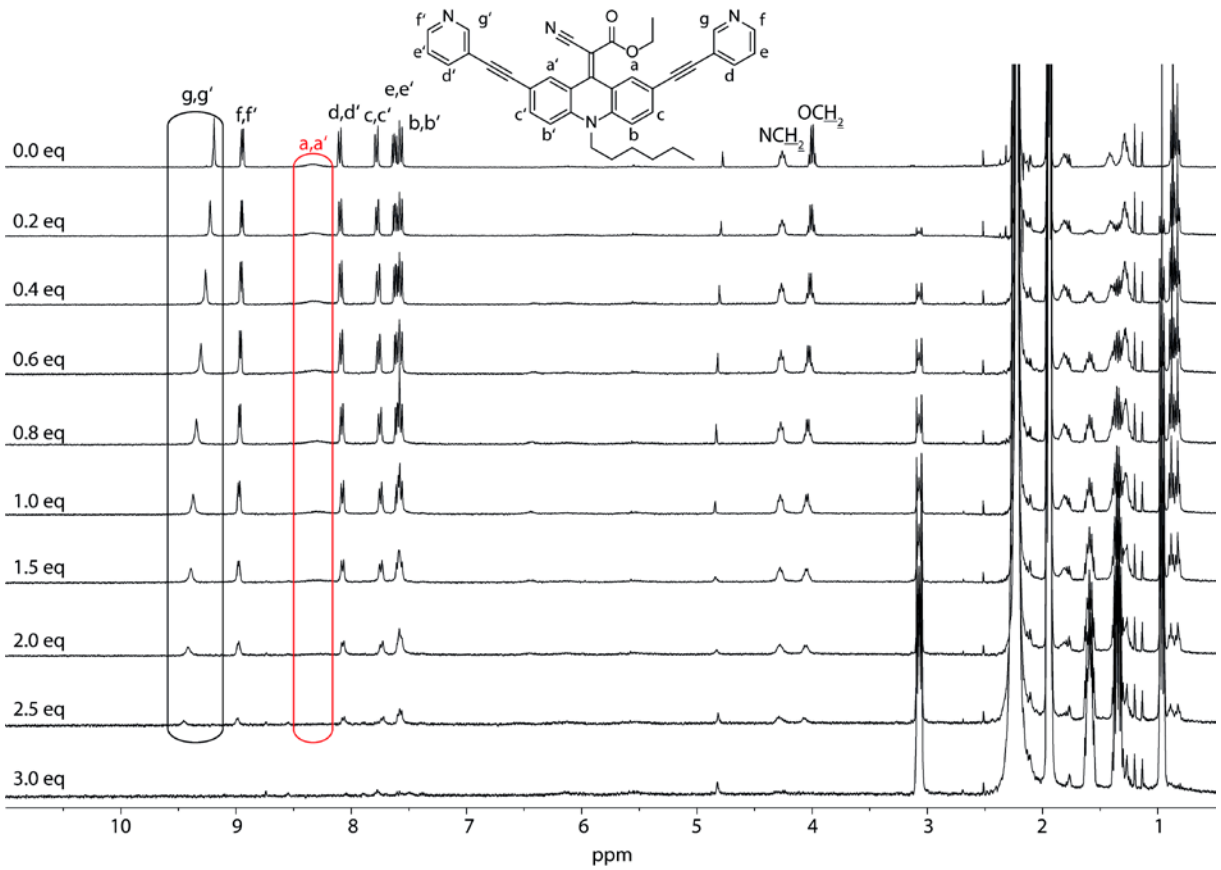


**Figure SI16** $^1$H NMR titration (400 MHz, 298 K, $CD_3CN$) of $[Pd_2\mathbf{L}^{Et}_4]$ with $(NBu_4)_2\mathbf{G}^4$. The chemical shifts of the inward pointing protons change gradually due to a fast exchange of the guest on the NMR time scale. Excess addition of $\mathbf{G}^4$ leads to precipitation of the cage.

### 3.1.5 Titration of $[Pd_2L^{Et}_4]$ cage with $G_5$

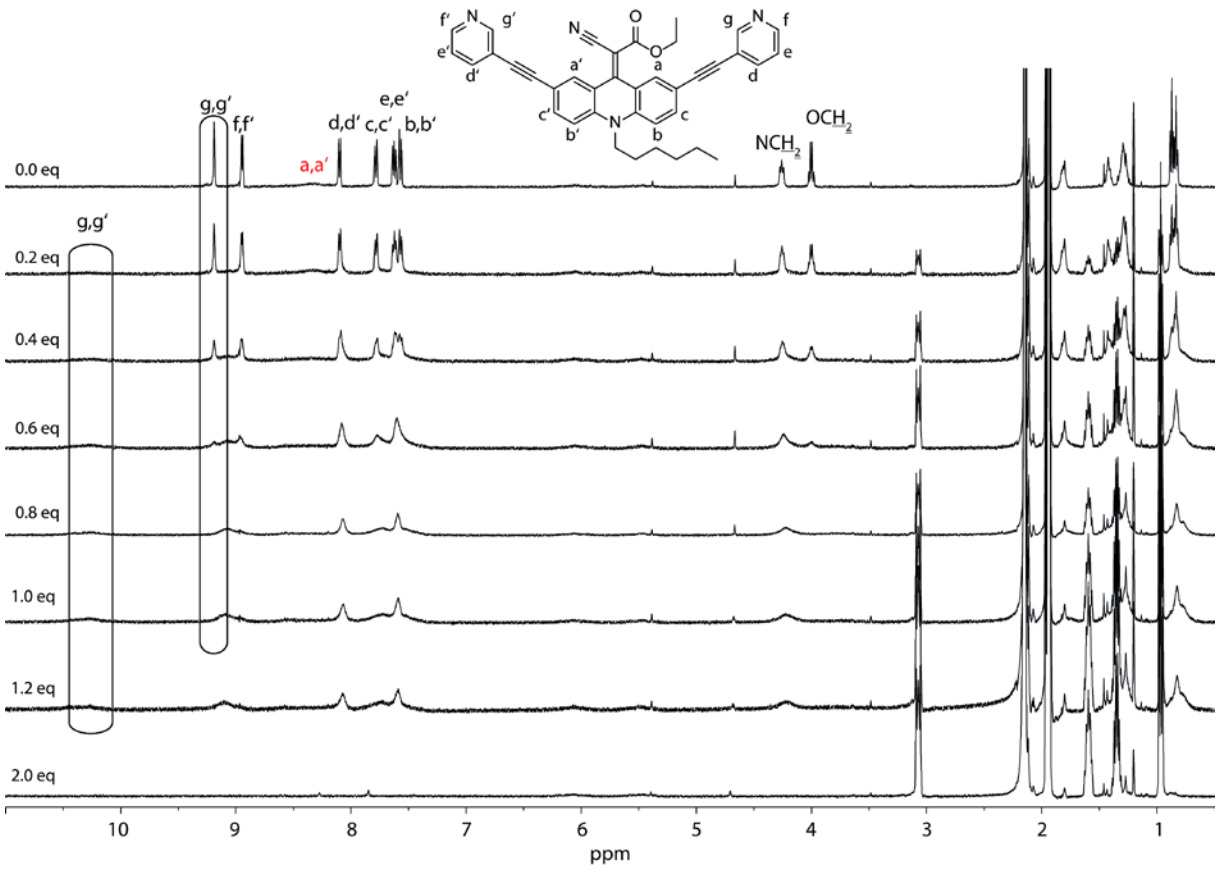


**Figure SI17** $^1$H NMR titration (400 MHz, 298 K, $CD_3CN$) of $[Pd_2\mathbf{L}^{Et}_4]$ with $(NBu_4)_2\mathbf{G}^5$. Upon addition of one equivalent of guest $\mathbf{G}^5$ the $[Pd_2\mathbf{L}^{Et}_4]$ cage transforms into $[\mathbf{G}^5@Pd_2\mathbf{L}^{Et}_4]$. Excess addition of $\mathbf{G}^5$ leads to precipitation of the cage.

## 3.2 Solvent and temperature influence on $G_5$@[$Pd_2L^{Et}_4$] host -guest complex

### 3.2.1 $G_5$@[$Pd_2L^{Et}_4$] host -guest complex in DMSO at rt

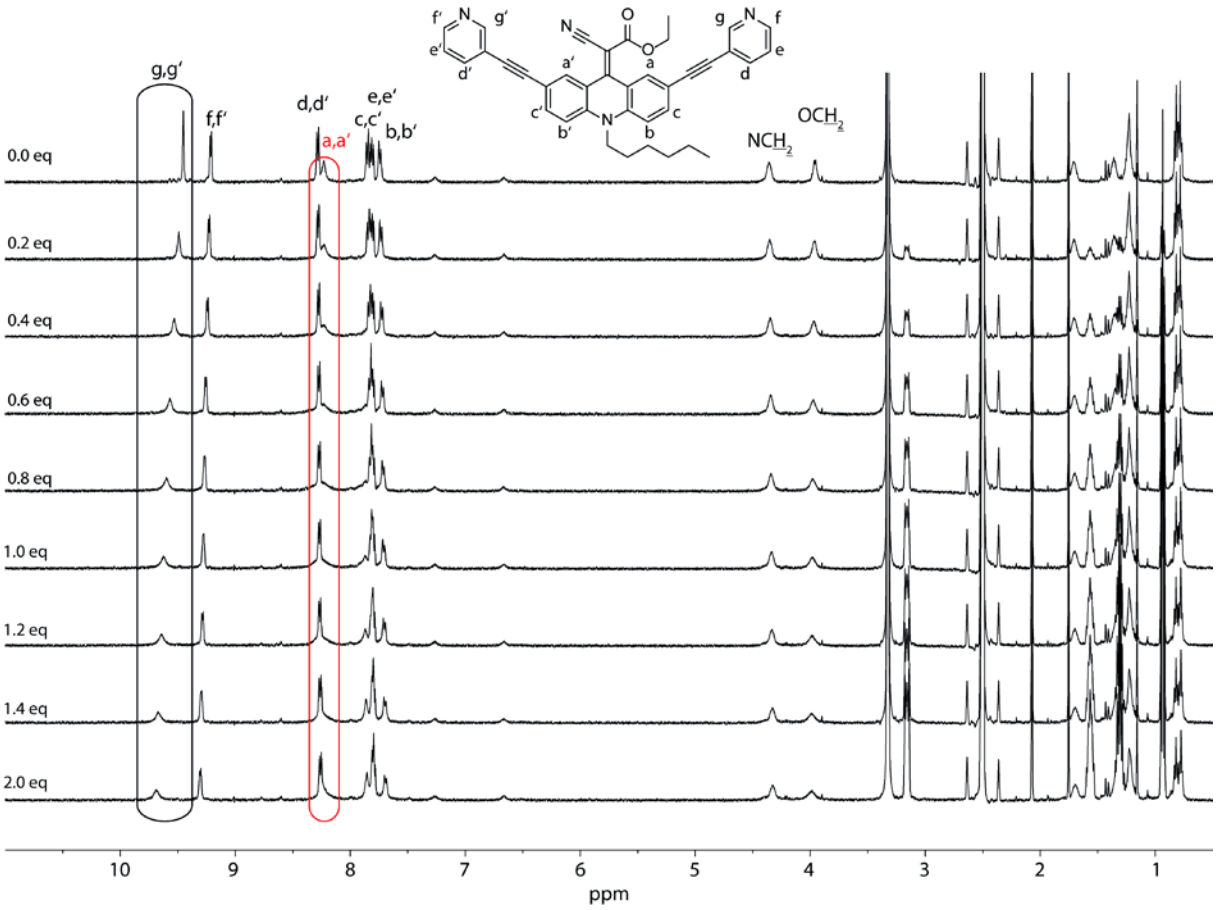


**Figure SI18** $^1$H NMR titration (400 MHz, 298 K, d$^6$-DMSO) of [$Pd_2\mathbf{L}^{\mathbf{Et}}_4$] with $(NBu_4)_2\mathbf{G}^{\mathbf{5}}$. The chemical shifts of the inward pointing protons change gradually due to a fast exchange of the guest on the NMR time scale. In contrast to the situation in $CD_3CN$ (Fig. SI12), in DMSO a fast exchange is observable for $G^5$ with [$Pd_2\mathbf{L}^{\mathbf{Et}}_4$].

### 3.2.2 Influence of solvent and temperature on host-guest complexes $G_5$@[$Pd_2L^{Et}_4$]

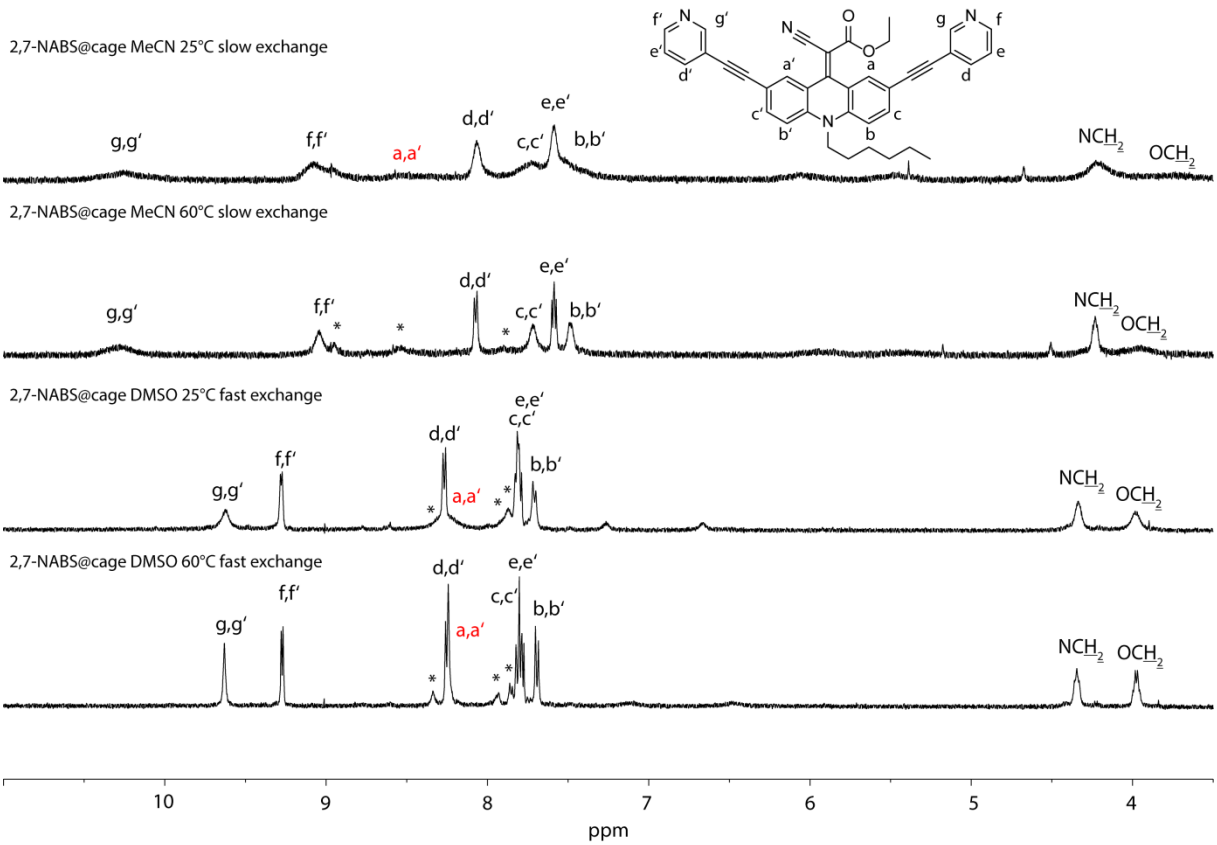


**Figure SI19** Comparison of $^1$H NMR spectra (400 MHz) of [$Pd_2\mathbf{L}^{\mathbf{Et}}_4$] with $(NBu_4)_2\mathbf{G}^{\mathbf{5}}$ in different solvents and at different temperatures.

### 3.2.3 $G_5$@[$Pd_2L^{Et}_4$] host-guest complex in MeOH at 60°C

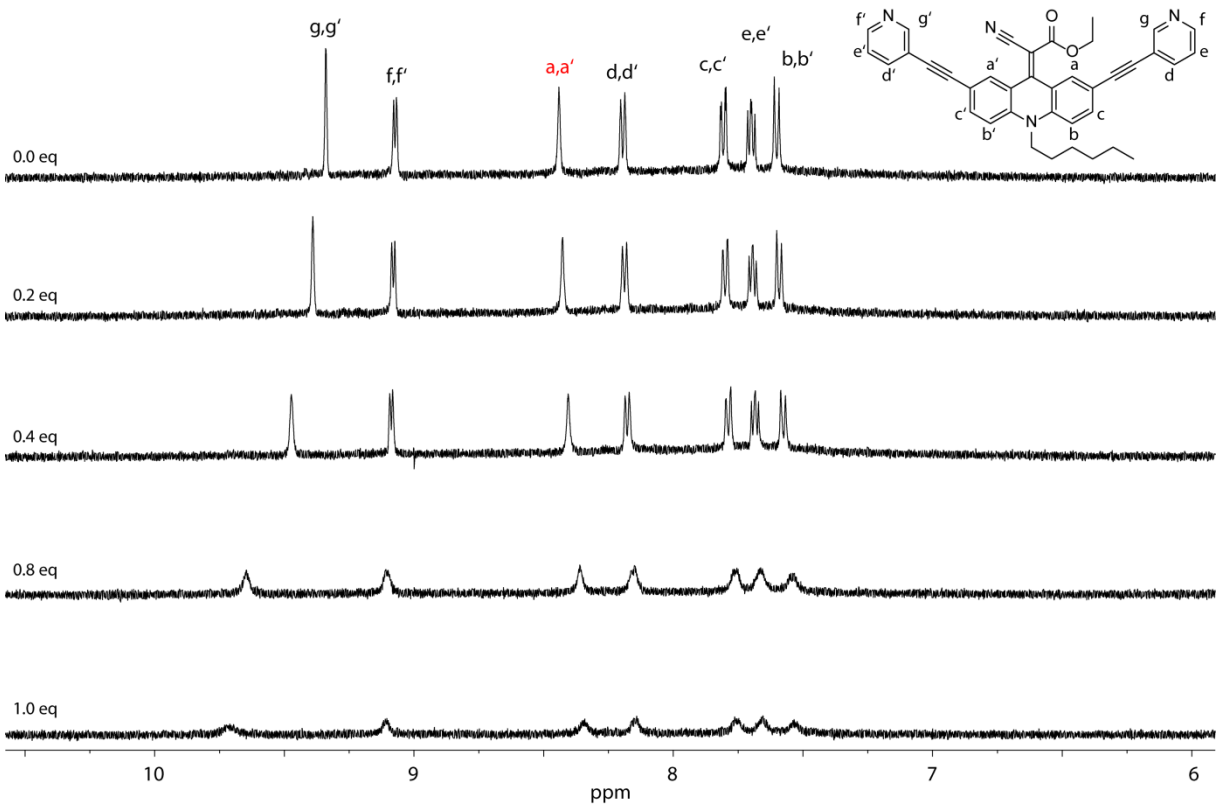


**Figure SI20** $^1$H NMR titration (400 MHz, 333 K, $CD_3OD$) of [$Pd_2\mathbf{L}^{Et}_4$] with $(NBu_4)_2\mathbf{G}^5$. The chemical shifts of the inward pointing protons change gradually due to a fast exchange of the guest on the NMR time scale. Addition of 0.4eq of $\mathbf{G}^5$ leads already to precipitation of the cage.

### 3.2.4 $G_5$@[$Pd_2L^{Et}_4$] host-guest complex in $MeNO_2$ at 60°C

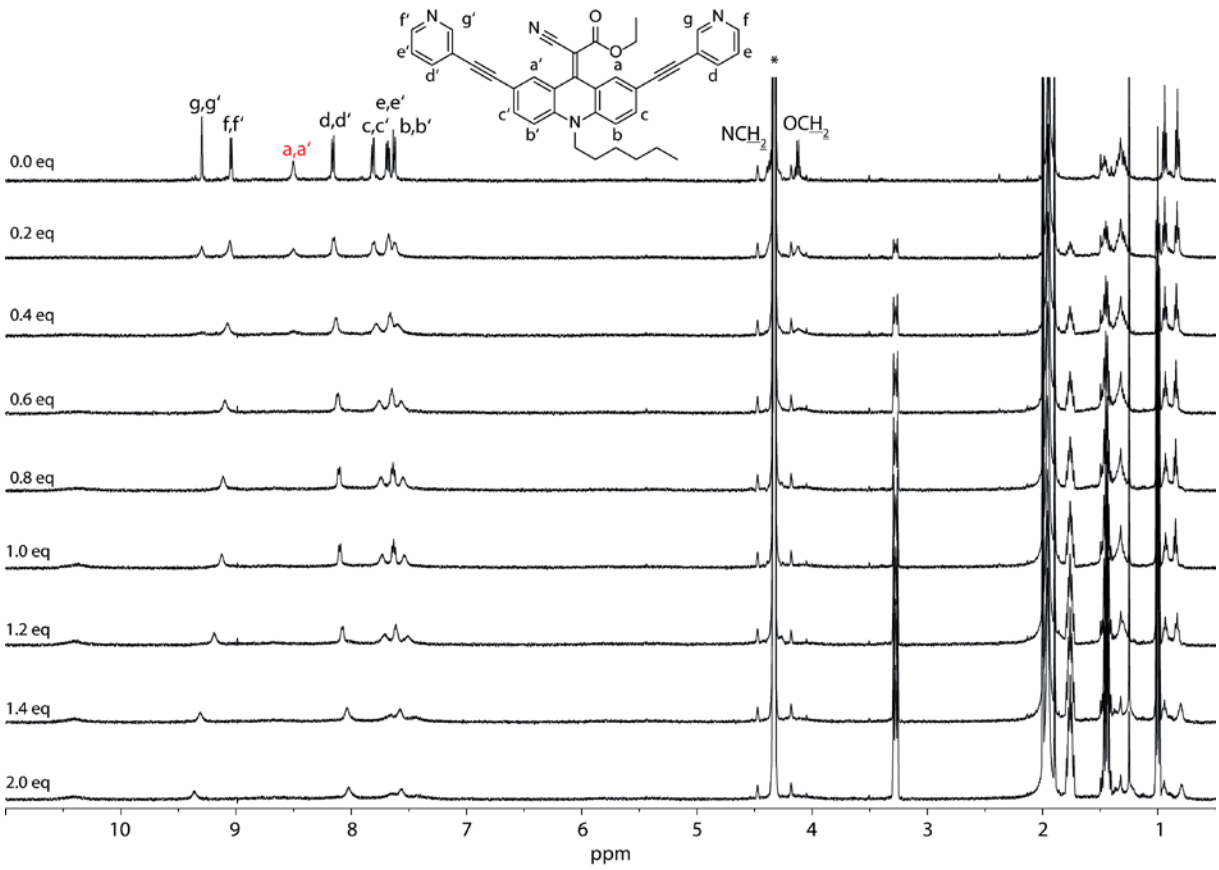


**Figure SI21** $^1$H NMR titration (400 MHz, 333 K, $CD_3NO_2$) of [$Pd_2\mathbf{L}^{Et}_4$] with $(NBu_4)_2\mathbf{G}^5$. Upon addition of one equivalent of guest $\mathbf{G}^5$ the [$Pd_2\mathbf{L}^{Et}_4$] cage transforms into [$\mathbf{G}^5$@$Pd_2\mathbf{L}^{Et}_4$]. Excess addition of $\mathbf{G}^5$ leads to precipitation of the cage.

### 3.2.5 $G_5$@[$Pd_2L^{Et}_4$] host-guest complex in DMSO at 60°C

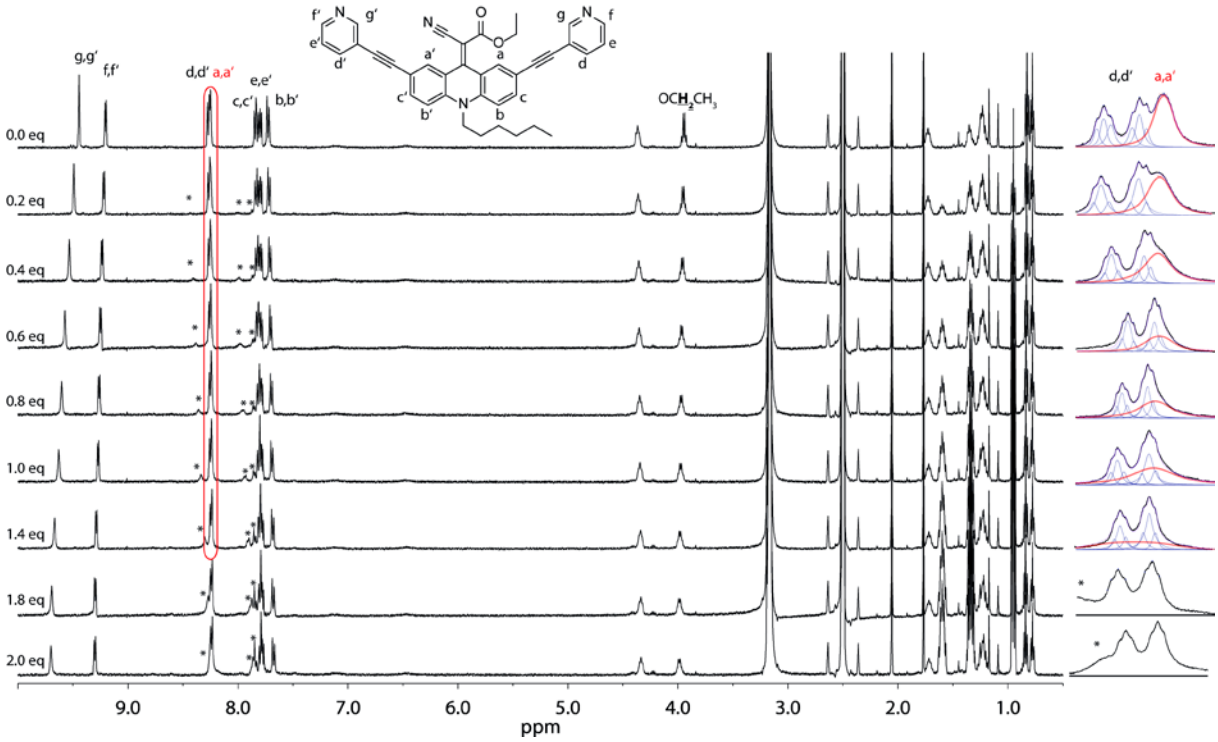


**Figure SI22** $^1$H NMR titration (400 MHz, 333 K, $d^6$-DMSO) of [$Pd_2\mathbf{L}^{\mathbf{Et}}_4$] with $(NBu_4)_2\mathbf{G}^{\mathbf{5}}$. The chemical shifts of the inward pointing protons change gradually due to a fast exchange of the guest on the NMR time scale. Guest signals are marked with *. On the right line fittings analyses of the deconvoluted signals d/d' and a/a' are shown. Whereas the d/d' signals do not broaden upon guest addition, the signal assigned to a/a' clearly broadens with increasing amounts of the guest which indicates that the encapsulated guest slows down the spinning of the rotors inside the cavity.

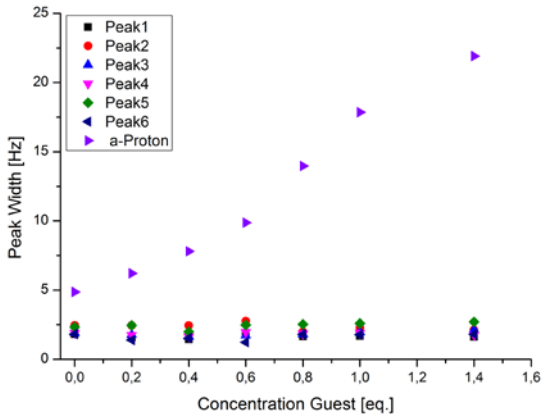


**Figure SI23** Correlation of peak width with the concentration of guest $G^5$ from line fitting analysis of the NMR titration data shown in Fig. SI13. Peaks 1-6 belong to the signal d/d' (1-6 from left to right), "a-proton" to the signal a/a'. The significant change of the a/a' signal peak width indicates a decrease of rotation rate upon guest uptake, while the peak width of other signals stays nearly constant.

# 4 X-Ray crystal structures

## 4.1 Table

| Structure | $L^{Et}$ | $L^{Ph}$ |
|---|---|---|
| CCDC number | 1478914 | 1478915 |
| Empirical formula | $C_{38}\ H_{32}\ N_4\ O_2$ | $C_{46}\ H_{32}\ D_8\ N_4\ O_3$ |
| Formula weight | 576.67 g $mol^{-1}$ | 704.87 g $mol^{-1}$ |
| Temperature | 100(2) K | 100(2) K |
| Wavelength | 0.71073 Å | 1.54178 Å |
| Crystal system | Monoclinic | Triclinic |
| Space group | *$P2_1/n$* | *P-1* |
| Unit cell dimensions | a = 11.4777(5) Å<br>b = 15.9325(7) Å<br>c = 17.0968(8) Å<br>Alpha = 90°<br>Beta = 103.233(2)°.<br>Gamma = 90° | a = 9.7141(3) Å<br>b = 13.7175(4) Å<br>c = 13.8642(4) Å<br>Alpha = 92.206(2)°.<br>Beta = 97.198(2)°.<br>Gamma = 98.744(2)°. |
| Volume | 3043.4(2) Å3 | 1808.46(9) $Å^3$ |
| Z | 4 | 2 |
| Density (calculated) | 1.259 Mg/m3 | 1.294 Mg/m3 |
| Absorption coefficient | 0.079 mm-1 | 0.638 $mm^{-1}$ |
| F(000) | 1216 | 736 |
| Crystal size | 0.844 x 0.744 x 0.542 mm3 | 0.300 x 0.116 x 0.072 $mm^3$ |
| Theta range for data collection | 2.331 to 33.141°. | 3.22 to 74.61°. |
| Index range | -17<=h<=17,<br>-23<=k<=24,<br>-26<=l<=23 | -12<=h<=12,<br>-17<=k<=17,<br>-17<=l<=17 |
| Reflections collected | 114976 | 21094 |
| Independent reflections | 11572 [R(int) = 0.0375] | 7238 [R(int) = 0.0382] |
| Completeness to theta | 99.5 % | 97.7 % |
| Refinement method | Full-matrix least-squares on F2 | Full-matrix least-squares on F2 |
| Data / restraints / parameters | 11572 / 0 / 399 | 7238 / 1 / 499 |
| Goodness-of-fit on F2 | 1.116 | 1.047 |
| Final R indices [I>2sigma(I)] | R1 = 0.0411,<br>wR2 = 0.1192 | R1 = 0.0477,<br>wR2 = 0.1094 |
| R indices (all data) | R1 = 0.0473,<br>wR2 = 0.1246 | R1 = 0.0643,<br>wR2 = 0.1183 |
| Largest diff. peak and hole | 0.829 and -0.284 e.Å-3 | 0.243 and -0.275 $e.Å^{-3}$ |

# 5 Computational Studies

In order to learn about the preferred conformation(s) of the assembled cages, we performed unconstrained DFT geometry optimizations at the B3LYP-D3/def2-SVP (PCM solvation: acetonitrile, charge+4, counter anions omitted) of several PM6-preoptimized starting geometries with different double-bond orientations using the software Gaussian '09.[4]

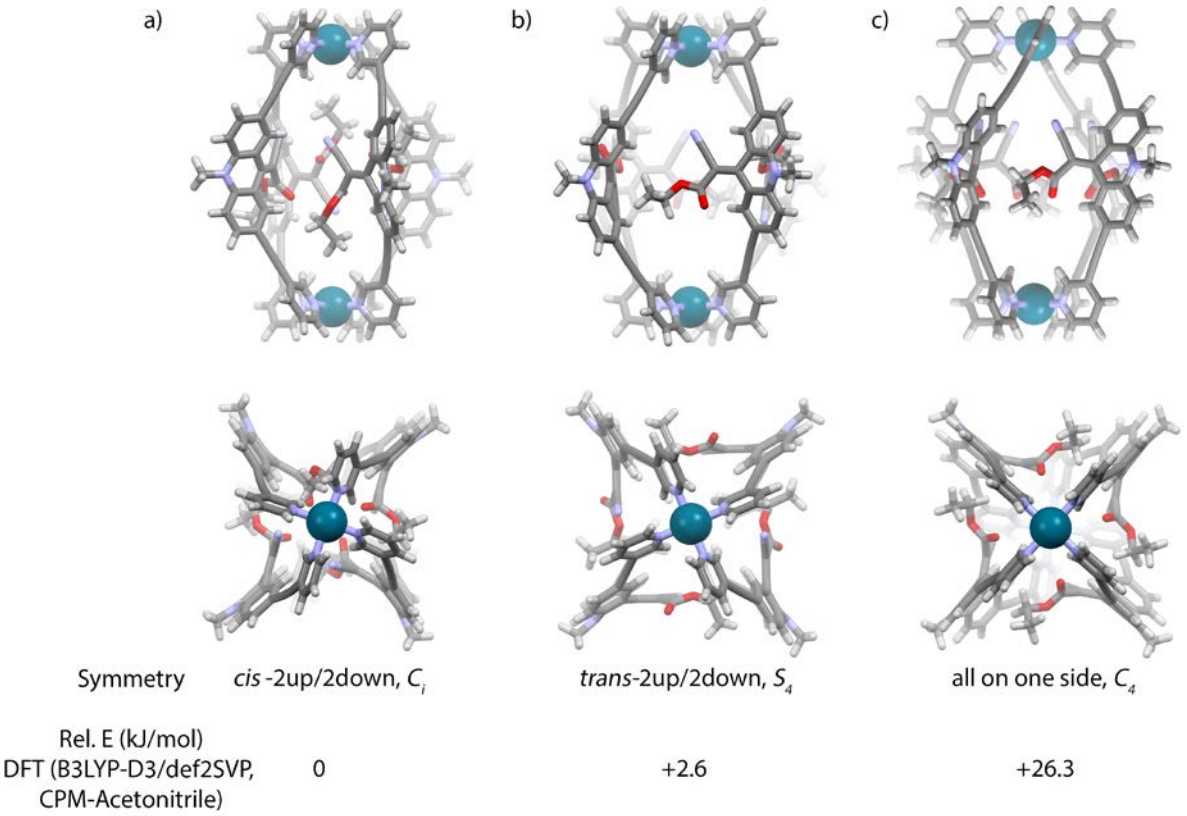


**Figure SI24** The calculations revealed that the (a) *cis*-2up/2down arrangement is energetically only slightly favoured over (b) the *trans*-2up/2down arrangement but both are much lower in energy than the sterically congested (c) all-on-one side geometry (a tentative 1up/3down arrangement was omitted from the calculations).

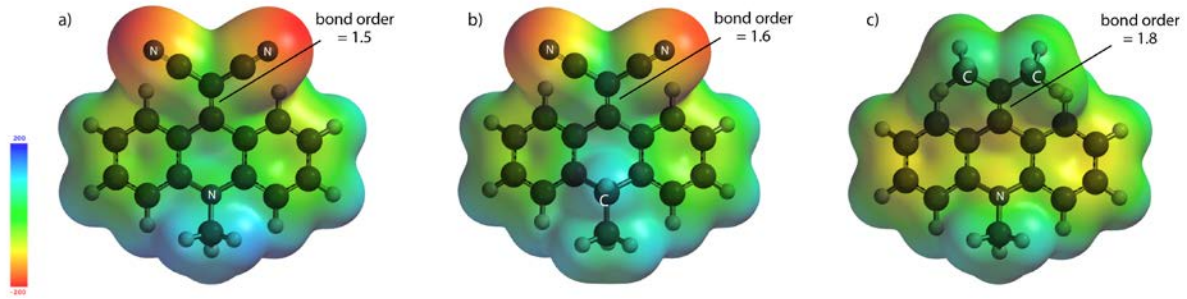


**Figure SI25** The influence of the electronic situation in the push-pull system on the relative distribution of the electrostatic potential and the bond-order of the double-bond was calculated on the DFT EDF2/6-31G(D) level of theory using the software Wavefunction Spartan '14.[6] (a) Backbone of ligand $\mathbf{L}^{\mathbf{CN}}$, (b) same with donor nitrogen exchanged for a $sp^3$ carbon, (c) same with acceptor nitriles exchanged for methyl groups.

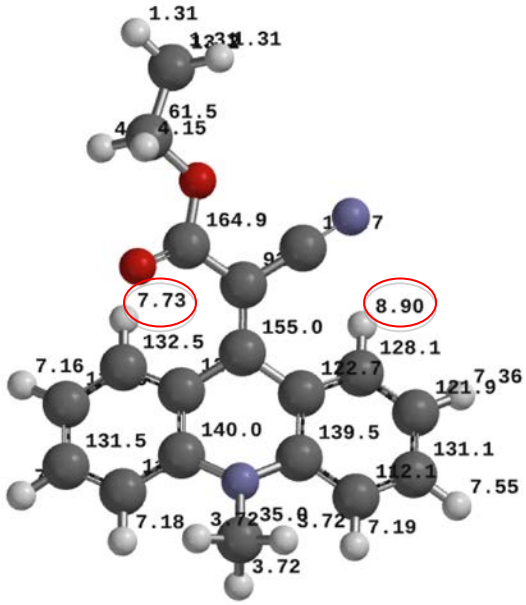


**Figure SI26** A rough calculation of the NMR chemical shifts at the DFT GIAO- EDF2/6-31G(D) level of theory using the software Wavefunction Spartan '14[7] indicates which of the a protons in the slow exchanging systems (at low temperatures) is expected to resonate at higher/lower field.


1 S. Löffler, J. Lübben, L. Krause, D. Stalke, B. Dittrich and G. H. Clever, *J. Am. Chem. Soc.*, 2015, **137**, 1060–1063.

2 F. Bureš, *RSC Adv.,* 2014, **4**, 58826–58851.

3 F. P. Gasparro, N. H. Kolodny, *J. Chem. Educ.,* 1977, **54**, 258-261.

4 SpinWorks 4.2.4, K. Marat, University of Manitoba, **2016.**

5 S. Löffler, J. Lübben, A. Wuttke, R. A. Mata, M. John, B. Dittrich and G. H. Clever, *Chem. Sci.*, 2016, DOI: 10.1039/C6SC00985A.

6 M. J. Frisch, G. W. Trucks, H. B. Schlegel, G. E. Scuseria, M. A. Robb, J. R. Cheeseman, G. Scalmani, V. Barone, B. Mennucci, G. A. Petersson, H. Nakatsuji, M. Caricato, X. Li, H. P. Hratchian, A. F. Izmaylov, J. Bloino, G. Zheng, J. L. Sonnenberg, M. Hada, M. Ehara, K. Toyota, R. Fukuda, J. Hasegawa, M. Ishida, T. Nakajima, Y. Honda, O. Kitao, H. Nakai, T. Vreven, J. A. Montgomery Jr., J. E. Peralta, F. Ogliaro, M. J. Bearpark, J. Heyd, E. N. Brothers, K. N. Kudin, V. N. Staroverov, R. Kobayashi, J. Normand, K. Raghavachari, A. P. Rendell, J. C. Burant, S. S. Iyengar, J. Tomasi, M. Cossi, N. Rega, N. J. Millam, M. Klene, J. E. Knox, J. B. Cross, V. Bakken, C. Adamo, J. Jaramillo, R. Gomperts, R. E. Stratmann, O. Yazyev, A. J. Austin, R. Cammi, C. Pomelli, J. W. Ochterski, R. L. Martin, K. Morokuma, V. G. Zakrzewski, G. A. Voth, P. Salvador, J. J. Dannenberg, S. Dapprich, A. D. Daniels, Ö. Farkas, J. B. Foresman, J. V. Ortiz, J. Cioslowski, D. J. Fox, Gaussian, Inc., Wallingford, CT, USA, **2009**.

7 Spartan '14 Version 1.2.0, Wavefunction, Inc., Irvine, CA, **2014**.